Climate Dynamics
https://doi.org/10.1007/s00382-021-05765-1

Observational analysis of decadal and long-term hydroclimate drivers in the Mediterranean region: role of the ocean–atmosphere system and anthropogenic forcing

Roberto Suárez-Moreno[1] · **Yochanan Kushnir**[1] · **Richard Seager**[1]

Received: 30 June 2020 / Accepted: 8 April 2021

Abstract
Using observations and reanalysis, we develop a robust statistical approach based on canonical correlation analysis (CCA) to explore the leading drivers of decadal and longer-term Mediterranean hydroclimate variability during the historical, half-year wet season. Accordingly, a series of CCA analyses are conducted with combined, multi-component large-scale drivers of Mediterranean precipitation and surface air temperatures. The results highlight the decadal-scale North Atlantic Oscillation (NAO) as the leading driver of hydroclimate variations across the Mediterranean basin. Markedly, the decadal variability of Atlantic-Mediterranean sea surface temperatures (SST), whose influence on the Mediterranean climate has so far been proposed as limited to the summer months, is found to enhance the NAO-induced hydroclimate response during the winter half-year season. As for the long-term, century scale trends, anthropogenic forcing, expressed in terms of the global SST warming (GW) signal, is robustly associated with basin-wide increase in surface air temperatures. Our analyses provide more detailed information than has heretofore been presented on the sub-seasonal evolution and spatial dependence of the large-scale climate variability in the Mediterranean region, separating the effects of natural variability and anthropogenic forcing, with the latter linked to a long-term drying of the region due to GW-induced local poleward shift of the subtropical dry zone. The physical understanding of these mechanisms is essential in order to improve model simulations and prediction of the decadal and longer hydroclimatic evolution in the Mediterranean area, which can help in developing adaptation strategies to mitigate the effect of climate variability and change on the vulnerable regional population.

Keywords Climate variability · Hydroclimate drivers · Sea surface temperatures · Atmospheric circulation · Anthropogenic forcing · Multivariate analysis

1 Introduction

The Mediterranean basin is a region of varied landscapes, ranging from coastal wetlands and semi-arid steppes to high mountains and deserts. The region experiences a wet season that extends from October to May, and a dry often hot and sultry summer from June to September (Kottek et al. 2006). It is frequented by droughts and water resources are often scarce. Climate models project a trend towards greater aridification of the Mediterranean region in response to rising greenhouse gases (GHGs), a trend that is detectable in observations (Somot et al. 2008; Kelley et al. 2012a, b; Seager et al. 2014, 2019; Zappa et al. 2015; Tang et al. 2018). According to the special report of the Intergovernmental Panel on Climate Change (IPCC 2018), the increase in global mean temperatures could, at the current rate of warming, reach 1.5 K and more before the mid-twenty-first century relative to the middle of the nineteenth century, leading to unprecedented climate-related risks and extreme weather events. Indeed, Zittis et al. (2019) point out that this warming rate has already been reached in the Mediterranean region, where temperatures are expected to increase by 20% more than the global average, and winter precipitation is

This paper is a contribution to the MEDSCOPE special issue on the drivers of variability and sources of predictability for the European and Mediterranean regions at subseasonal to multi-annual time scales. MEDSCOPE is an ERA4CS project co-funded by JPI Climate. The special issue was coordinated by Silvio Gualdi and Lauriane Batté.

✉ Roberto Suárez-Moreno
rsuarez@ldeo.columbia.edu

[1] Lamont-Doherty Earth Observatory, Columbia University, Palisades, NY, USA

Published online: 24 April 2021

projected to decrease by as much as 7 mm/K in the central and southern areas (Lionello and Scarascia 2018). Moreover, the Mediterranean region is an area of social and political instability, human migration and, in the Middle East, open violent conflict. Though the main drivers of Mediterranean migration patterns are primarily economic and political, climate change and environmental stress may play an indirect or subsidiary role (De Haas 2011; Kelley et al. 2015; Cramer et al. 2018).

As proposed in a series of works based on both observations and simulations with general circulation models (GCMs), the Hadley circulation widens and weakens under global warming (GW), causing a poleward shift of the subtropical dry zone in both hemispheres (Hu and Fu 2007; Gastineau et al. 2008; Hu et al. 2013). In a recent analysis, Grise et al. (2019) showed that tropical expansion in atmospheric reanalyses is consistent with that simulated by Coupled Model Intercomparison Project Five (CMIP5) models. The latter show an emerging agreement that both increasing GHGs and stratospheric ozone depletion contributed to the widening of the Hadley circulation during the late twentieth century, and that the expansion trend will continue as GHGs keep increasing, although ozone recovery will oppose this in the southern hemisphere (Lu et al. 2007; Tao et al. 2016; Grise et al. 2019). In the northern hemisphere, the GHG-induced tropical expansion to date is considerably smaller than in the Southern Hemisphere, remaining difficult to detect under a background of large natural variability (Grise et al. 2019). Thus, identifying the poleward shift of the descending branch of the Hadley circulation and how it would affect the climate in the Mediterranean region might be complicated.

On decadal time scales, climate variability in the Euro-Mediterranean region is primarily governed by the North Atlantic Oscillation (NAO). The NAO is the most prominent mode of multi-scale, internal variability in the North Atlantic sector. The spatial pattern of the NAO depicts a north–south oscillation in atmospheric mass, with pressure centers over Iceland and the subtropical Atlantic and Iberian Peninsula (Hurrell 1995; Jones et al. 1997) that drives large-scale atmospheric circulation variability from the polar to subtropical Atlantic and adjacent continental landmasses (e.g., Hurrell et al. 2001, 2003; Visbeck et al. 2001; Hurrell and Deser 2009). The NAO is more pronounced during boreal winter, modulating the direction and strength of westerly winds, the intensity and frequency of storms, heat and moisture transport (Seager et al. 2020). However, the origins of NAO decadal and longer-term variability are not well understood and are subject to constant debate.

Relevant to the scope of this work is the decadal-scale NAO variability (hereinafter DNAO). The DNAO has been proposed to lead oceanic Atlantic multidecadal SST variability (AMV) during the observed record (Li et al. 2013; McCarthy et al. 2015). The conjectured mechanism suggests ocean–atmosphere interaction and oscillatory behavior on multidecadal time scales (e.g., Visbeck et al. 2003; Sun et al. 2015; Delworth et al. 2017), even though observational evidence for this behavior is tenuous. In any case, regardless of the underlying mechanism of this hypothetical DNAO-AMV feedback, the merged effect of both phenomena on the Mediterranean hydroclimate has not been addressed so far. Often referred to as the Atlantic Multidecadal Oscillation (AMO), the AMV is expressed as decadal-to-multidecadal, basin-wide, spatially-uniform North Atlantic SST variability (e.g., Kushnir 1994; Schelsinger and Ramankutti 1994; Enfield et al. 2001; Ting et al. 2009). The AMV has been linked to low-frequency hydroclimate variability in Europe, North America, Africa and even India (Sutton and Hodson 2005; Knight et al. 2006; Zhang et al. 2007; Sutton and Dong 2012; Ghosh et al. 2017; O'Reilly et al. 2017; Qasmi et al. 2017; Ruprich-Robert et al. 2017; Zampieri et al. 2017; Årthun et al. 2018), albeit its influence on Mediterranean rainfall and surface air temperatures is mostly restricted to summer, even though the AMV impact on winter temperatures in the eastern Mediterranean and Middle-East has been conjectured (Ting et al. 2011).

Beyond AMV, it has been suggested that decadal SST variations in the Mediterranean Sea and Pacific Ocean can impact the North Atlantic-Europe atmospheric circulation. Idealized SST anomalies (SSTA) prescribed in the Mediterranean Sea in a GCM generates a circumglobal teleconnection that induces anomalous DNAO conditions (Li 2006; García-Serrano et al. 2013). That said and as far as decadal variability is concerned, it should be noted that Mediterranean SSTA have been proposed to be dynamically induced by the AMV through atmospheric processes (e.g., Marullo et al. 2011; Mariotti and Dell'Aquila 2012; Ruprich-Robert et al. 2017). Regarding the Pacific Ocean, decadal SST variability is dominated by the Interdecadal Pacific Oscillation (IPO), a large-scale, long period oscillation of SSTs that is seen as the decadal expression of the El Niño-Southern Oscillation (ENSO) phenomenon (e.g., Meehl et al. 2013; Zhang et al. 2019). The discussion of the influence of IPO on the Mediterranean ocean–atmosphere system is limited to a few observational studies. Multidecadal variability of winter cyclones in the Mediterranean region was shown to fluctuate according to IPO-induced changes in the large-scale atmospheric circulation over the North Atlantic (Maslova et al. 2017). In other works, the combined effects of the IPO and El Niño-Southern Oscillation (ENSO) were linked to global hydroclimate variability in general, and Mediterranean wet-dry changes in particular (Mariotti et al. 2002, 2005; Wang et al. 2014). Finally, Dong and Dai (2015) used observations, reanalysis products and model simulations to analyze the IPO influence on temperature and precipitation worldwide,

finding a negative correlation with surface air temperatures across the Mediterranean-Middle East.

In summary, the origin of the large-scale atmospheric circulation that determines decadal hydroclimate variability in the Mediterranean region during the half-year wet season is not well known. It might be internal atmospheric variability, with the DNAO playing an outstanding role, or it could arise from ocean–atmosphere interactions, within which the AMV, IPO and Mediterranean Sea decadal SST variability play a role. However, the effects of these phenomena on the Mediterranean climate have been addressed separately, so any combined effect would have been overlooked. On longer time scales, it will be necessary to characterize and quantify this marked natural variability in order to detect and isolate the anthropogenic forced trend in the Mediterranean region, as well as the associated hypothesized northward expansion of the Hadley cell.

Motivated by the uncertainties raised above, we use a multivariate analysis method based on canonical correlation analysis (CCA) to robustly explore the leading decadal-to-long-term drivers of Mediterranean hydroclimate variability. The CCA method has been applied in previous studies to investigate the main coupled circulation-rainfall patterns in the Mediterranean region on decadal and longer time scales. These studies focused on relating large-scale atmospheric circulation at different tropospheric levels to the variability and trends of Mediterranean precipitation during the second half of the twentieth century (Dünkeloh and Jacobeit 2003; Xoplaki et al. 2004). In a similar context, Mariotti and Dell'Aquila (2012) used linear correlation applied to observational datasets spanning the period 1850–2009 to explore large-scale forcings of decadal climate variability in the Mediterranean area. Distinctively, our CCA analyses are conducted in a novel way with combined, multi-component large-scale drivers of Mediterranean precipitation and surface air temperatures to evaluate the effects of large-scale atmosphere variability, SST variability and anthropogenic forcing on precipitation and surface air temperatures in 3-month periods covering the half year (October-to-March) wet season. On the one hand, the results of this work corroborate the expected rising trend of winter temperatures under anthropogenic forcing and the dominant role of DNAO-related natural variability when it comes to precipitation during the winter peak season. On the other hand, our key findings show an outstanding role for AMV in enhancing the impact of DNAO on winter precipitation and surface air temperatures that would have been overlooked so far. Furthermore, our results denote a GW-induced drying trend in accordance with the projected GHGs-forced aridification of the Mediterranean region, showing that a local northward shift of the subtropical dry zone over the basin is in process.

The study is structured as follows. Section 2 is devoted to data and methodology, presenting the statistical approach that gives rise to the results shown later in Sect. 3. Finally, the conclusions and discussion are presented in Sect. 4.

2 Data and methods

2.1 Data

We use precipitation and surface air temperatures data (hereinafter PCP and TEMP respectively) from the Climate Research Unit (CRU) Time-Series (TS) version 4.02 of high resolution ($0.5° \times 0.5°$) gridded monthly data, spanning the period 1901–2017 (Harris et al. 2020). Due to observational uncertainty in the Mediterranean region, particularly for precipitation (Zittis 2018), CCA analysis was also performed using high resolution ($0.5° \times 0.5°$) data from the Full data Reanalysis of the Global Precipitation Climatology Centre (GPCC; Schneider et al. 2013). The results found do not differ significantly from those corresponding to CRU, which are presented in this work.

For SST, we use version 5 of the Extended Reconstructed Sea Surface Temperature (ERSST) dataset from the National Oceanic and Atmospheric Administration (NOAA). The ERSST v5 is derived from the International Comprehensive Ocean–Atmosphere Dataset (ICOADS), and is presented on a $2.0° \times 2.0°$ grid with spatial completeness enhanced by statistical methods (see Huang et al. 2017 for extended details).

To examine circulation variability we use version 3 of the NOAA–CIRES–DOE Twentieth Century Reanalysis (20CRv3). This reanalysis uses a state-of-the-art data assimilation system applied to surface observations of synoptic pressure within NOAA's Global Forecast System with prescribed sea ice distribution and SST. The 20CR uses an ensemble filter data assimilation technique which directly estimates the most likely state of the global atmosphere for each 3-h period, also estimating uncertainty in the reanalysis. The most recent version used in this work (V3), provides 8-times daily estimates of global tropospheric variability across $1.0° \times 1.0°$ grids, covering 1836–2015 (Compo et al. 2011; Slivinski et al. 2019) and solves some data problems found in previous versions. Here we use surface pressure, sea level pressure (SLP), geopotential heights, horizontal wind components and specific humidity. The core of our analysis is based on SLP, being a reliable parameter because of the aforementioned assimilation procedure. Results based on other parameters should be interpreted more cautiously.

Additional calculations are performed from reanalysis variables. The low-level atmospheric thickness is computed as the difference in geopotential height between the 700 and 850 hPa pressure levels. The moisture transport is computed as the product of horizontal wind components $\left(V_h\right)$ and specific humidity (q), whereas the mean flow moisture

flux convergence (MFC) is calculated at each pressure level as follows:

$$MFC = -\nabla \cdot \left(qV_h\right) = -V_h \cdot \nabla q - q\nabla \cdot V_h \quad (1)$$

where $\nabla = \hat{i}(\partial/\partial x) + \hat{j}(\partial/\partial y)$ and $V_h = (u, v)$. In Eq. (1), the first and second terms to the right are calculated separately and represent the horizontal advection of specific humidity and the product of the specific humidity and horizontal mass convergence respectively (i.e., advection and convergence terms of MFC). Positive (negative) values indicate moisture convergence (divergence). The terms related to MFC and moisture transport are vertically integrated between the 200 and 1000 hPa pressure levels following the trapezoidal method. Likewise, thermal advection is calculated at each pressure level as:

$$-\nabla \cdot \left(TV_h\right) = -V_h \cdot \nabla T - T\nabla \cdot V_h \quad (2)$$

The thermal advection is vertically integrated between the 700 and 850 hPa pressure levels. Finally, we quantify the strength and geometry of the Hadley circulation in terms of the mean meridional mass stream function (see e.g., Cook 2004 for detailed explanation). In all cases, we refer to anomalies calculated as departures from the climatological mean. For the best evaluation of decadal variability and long-term trends, we focus on the longest period common to the datasets used, namely 1901–2015. Nonetheless, the calculations were also performed from 1921 onwards owing to uncertainties in rainfall observations for the first decades of the twentieth century. These uncertainties are likely related to fewer precipitation observations during the early twentieth century and the reliance on diverse methods to fill in these gaps in the different observational datasets (see Sun et al. 2018). The results found did not differ significantly from the longer period exposed herein.

2.2 Canonical correlation analysis

CCA is a widely used statistical method intended to identify maximally correlated time and space features between two multivariate, random variables, of which one is designated as explanatory and the other as the response. Analytical passage of this methodology in a multidisciplinary context can be found in Thompson (2000) among others. This multivariate analysis identifies a number of independent "canonical modes" that are linear combinations of the explanatory variables (EVs) and the response variables (RVs), respectively, which maximize the linear correlation between them (e.g., Green 1978; Green and Carroll 1978). A review of concepts that appear recurrently throughout this work and are essential for mechanistic interpretation of the results is provided in Appendix 1.

In climate studies, CCA is often applied when seeking the relationship between two time varying, space dependent fields, e.g., SST and SLP. Based on physical consideration and the direction of assumed causality, one of these fields may be considered explanatory (EV) and the other the response (RV). CCA then seeks to identify patterns within the explanatory field that best correlate (and explain) select patterns of variability in the response field. Because climate fields are spatially overdetermined (that is their space dimension does not represent their true number of degrees of freedom) it is customary to represent each field in the truncated space of their leading space-dependent empirical orthogonal functions (EOFs) and corresponding Principal Components (PCs) time series (e.g., Barnett and Preisendorfer 1987). The procedure then applies singular value decomposition (SVD) to the covariance matrix between the two sets of PCs. In this framework, CCA and SVD are intended as approaches for estimating a time series from a time-dependent vector and vice versa, and can be associated with climate variability in terms of regression maps (see full analytical development in Widmann 2005). The left and right matrices that solve the diagonalization of the covariance matrix provide the coefficients needed to calculate the left and right canonical variate, which are the linear combination of the left (EV) field PCs that best correlate with the corresponding linear combination of the right (RV) field PCs. The resulting pairs of canonical variates are independent of one another and are mutually orthogonal (for extended description and an algebraic representation of the procedure see Barnett and Preisendorfer 1987; Bretherton et al. 1992; Wilks 1995 and Hair et al. 2010 among others). The success of this method depends on the selection of the variables and the PCA truncation. Unlike its usual application, we use CCA in a novel way to explore the contributions of individual EVs (or a combination thereof) when the EV set is not composed of PCs for the same field, but are a series of time-dependent, multi-component indices of ocean–atmosphere variability known to influence the Mediterranean hydroclimate (see Sect. 1).

Specifically, we quantify and qualify the roles of (i) decadal atmospheric variability, (ii) decadal SST variability associated with the Atlantic (AMV), Pacific (IPO) and Mediterranean Sea (MED) basins, and (iii) anthropogenic forcing (i.e., the GW-induced change, represented by globally averaged SST). The EV set is thus constructed from the leading PCs of SLP in the North Atlantic-Europe-Mediterranean sector along with PCs calculated from SST, and the GW index. The guidelines to assess the contributions of individual EVs are detailed in Appendix 2.

It is important to recall that CCA is a multivariate regression technique to maximize correlation. Therefore, linear dependencies among individual EVs, the so-called multicollinearity, can obscure the weight of individual contributions,

limiting or impeding their interpretation. Multicollinearity is avoided when only PCs of a given field are used within a set of variables since, by construction, the EOFs retain orthogonality (i.e., all variables come from the truncated EOF space). Otherwise, multicollinearity among a given set of variables will confound the ability of the technique to isolate the contribution of any single variable, making its interpretation less reliable. Consequently, we need to examine multicollinearity within EVs before applying the CCA. This is done using the variance inflation factors (VIF) method (see Appendix 3).

3 Explanatory variables (EV)

Since atmospheric circulation variability, especially the DNAO, is known to play the dominant role in driving the Mediterranean climate, the leading SLP PCs in the North Atlantic-Europe-Mediterranean sector are part of the EV set. Regarding oceanic EVs, we select the leading PCs of SST in order to obtain the AMO, IPO and MED indices. To determine these SST-based time series we first calculate the GW index using yearly averaged global SST between 45°S and 60°N, due to low SST data coverage outside this latitude band (e.g., Baines and Folland 2007; Deser et al. 2010). In this way we intend to more precisely attribute surface air temperatures and precipitation anomalies in the Mediterranean region to internal atmospheric variability, SST variability and anthropogenic forcing, or a combination thereof. Yearly averages are calculated from July to June to be centered in the winter half-year study period (October-to-March). To highlight the low-frequency, secular trend in the GW index, the resulting time series is filtered using a low-pass Butterworth filter (order 4) with a cut-off period of 40 years. The Mann constraint of minimum slope is applied to account for trends at boundaries. This method reflects horizontally the time series at the extremes and can be overly conservative regarding trends (Mann 2004, 2008). The Mann method is used throughout this study each time a low-pass filter is applied. The resulting GW index is a good approximation to the observed, externally forced GHGs signal (Ting et al. 2009). As in previous studies, the GW effect on regional SST anomalies is then removed from the yearly SST field by regressing out the GW index at each grid point to obtain the residual SSTA. Since the impact of GW on SST is not spatially uniform, the first step consists in regressing the yearly SSTA onto the GW index:

$$SSTApat_i = \sum SSTA_i^j \cdot GW^j \tag{3}$$

where i is the spatial index that defines each grid point, j is the time index (number of years), $SSTA_i^j$ is the original SST field, GW^j is the GW index calculated as shown above, and $SSTApat_i^k$ is the GW-induced SSTA pattern between 45°S and 60°N, which serve to weight the residual SSTA calculation at each grid point, so that for each year, the SSTA pattern times the GW time series is subtracted from the original SSTA to define the SSTA residue:

$$SSTAres_i = SSTA_i^j - SSTApat_i \cdot GW^j \tag{4}$$

Next, and prior to EOF analysis, a low-pass Butterworth filter (fourth order) with a 10-year cut-off period is applied to the non-standardized residual SSTA to remove interannual variability. This methodology was previously applied in Trenberth and Shea (2006) and Mohino et al. (2011, 2016). Extended details can be found in those works. The results shown henceforth are not sensitive to the exact low-frequency cut-off period. The EOF analysis is then applied to the covariance matrix of time-filtered residual SSTA separately over the Atlantic (excluding the Mediterranean Sea) and Pacific Ocean basins, and the Mediterranean Sea. The PCs associated with these leading EOFs correspond to the AMO, IPO and MED indices (Fig. 1a), explaining 30, 30 and 75% of SST variance for the Atlantic and Pacific Oceans and the Mediterranean Sea, respectively. The spatial SST patterns associated with AMO, IPO, MED and GW are calculated by regression of residual SSTA onto their corresponding indices (Fig. 1b–e).

The PCs time series of SLP are calculated over the sector 70 W–60 E and 20–80 N. The longitudinal range is extended with respect to that often used for NAO definitions to cover a greater eastern extension that completely encompasses the Mediterranean region of study. In the same way it was done for the SST field, we calculate the SLP residual field by regressing out the GW-related SLP trend. In this case, calculations are performed for the winter half-year (October-to-March). We consider four SLP PCs that in combination retain 79% of decadal SLP variance (Fig. 2a) and 47, 13, 11 and 8% individually. Their associated spatial patterns are calculated by regression of the residual SLP field onto the PCs (Fig. 2b–e). The leading EOF (PC1) is identified as the DNAO (Fig. 2b). The decadal October-to-March station-based indices of the NAO following Hurrell (1995) and Jones et al. (1997) were compared with the DNAO signal computed here and had correlations of 0.79 and 0.81 respectively, significant at the 0.05 level under Ebisuzaki testing (Ebisuzaki 1997). The DNAO and the other SLP PCs represent decadal atmospheric circulation variability within the EV set that influence Mediterranean hydroclimate.

The time series of the four leading PCs of SLP are placed together with the AMO, IPO, MED and GW indices as columns of the EV matrix. Next, to assess multicollinearity within the EV set, we use the VIF method (see Appendix 3). Briefly, the closer the VIF value is to 1.0, the lower the linear dependence between individual variables or a combination thereof (e.g., Zuur et al. 2010). As expected (e.g., Marullo et al. 2011), the VIF reaches a

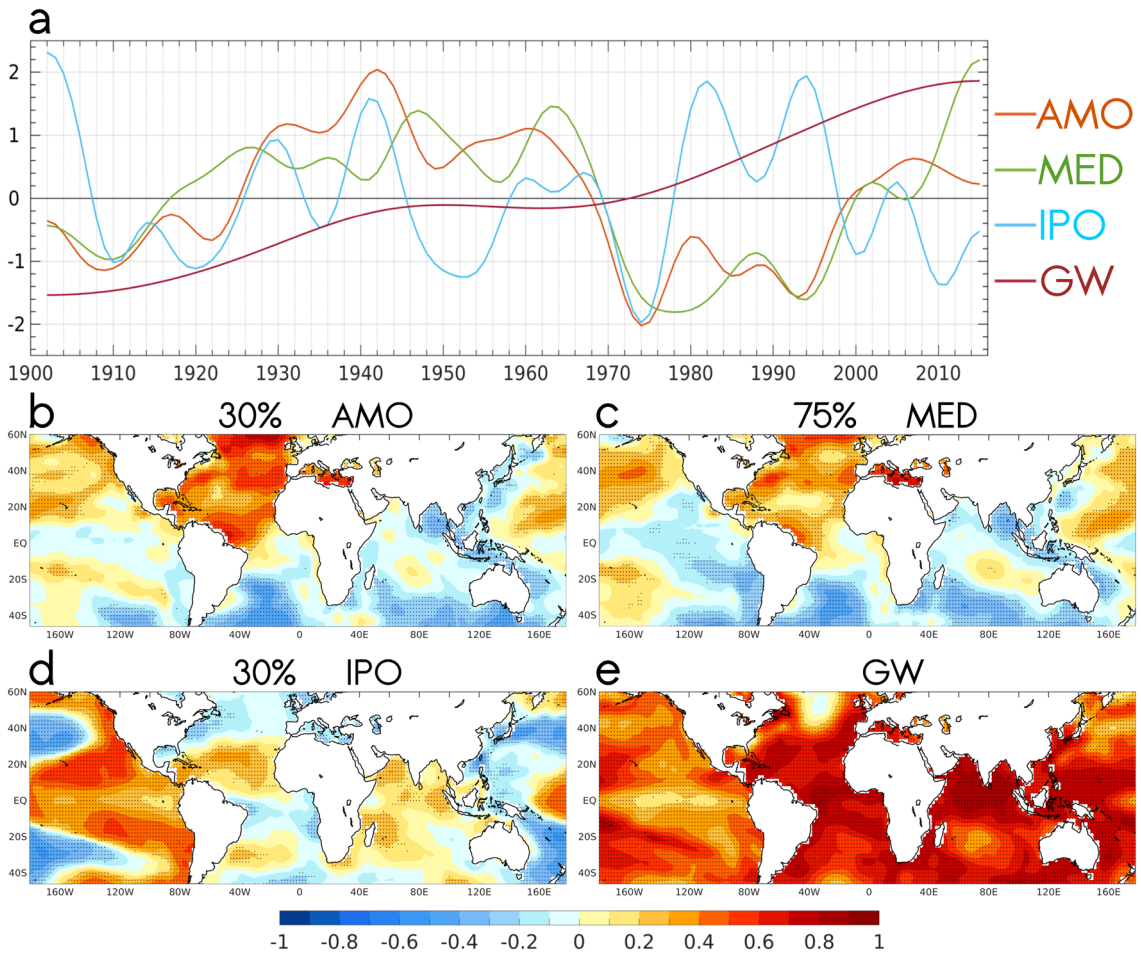

Fig. 1 Indices of decadal SST variability (PCs) and their associated spatial patterns calculated from the leading empirical orthogonal functions (EOFs). EOF analysis is applied over low-frequency filtered (using a low-pass Butterworth filter with a 10-year cutoff period) anomalies of residual SST in each independent ocean basin. The GW index is calculated on the globally averaged SST between 45S and 60 N and serves to estimate residual SST (see details on calculations in Sect. 2.3). **a** The 1901–2015 standardized AMV (orange line), MED (green line), IPO (blue line) and GW (burgundy line) indices obtained with ERSSTv5 data set. **b** SST (K std^{-1}) pattern calculated as the regression of anomalous residual ERSSTv5 onto the AMV index. (**c**) As for (**b**) but for the MED index. **d** As for (**b**) but for the IPO index. **e** GW pattern calculated as the regression of the GW index onto anomalous (non-residual) ERSSTv5. The percentages of explained variance from EOF analysis are 30, 75 and 30% for AMV, MED and IPO respectively

value of 6.33, which is the result of high and significant correlation (0.78) between the AMV and MED time series. Consequently, the information in the AMV and MED time series can be considered redundant. Thus, applying VIF analysis to the EV set after removing either AMV or MED indices provides values of 3.31 and 1.84 respectively. Therefore, due to closer linear independence (i.e., a VIF value closer to 1.0), we use the MED index as the explanatory variable that represents Atlantic-Mediterranean decadal SST variability, renaming the index and its associated SST pattern as AMDV hereinafter. The results in case of selecting the AMV index as representative of the leading SST variability in the Atlantic-Mediterranean sector reproduce those shown here. The EV set is thus composed of the four leading SLP PCs in the North Atlantic-Europe-Mediterranean region along with the AMDV, IPO and GW indices.

3.1 Response variables (RV)

The RV set is defined using an EOF analysis of Mediterranean (10 W–45E, 30–45 N) PCP and TEMP during the time-evolving, overlapping 3-month intervals from the summer-to-autumn, i.e., August–September-October (ASO), followed by September–October-November (SON) and so forth up to March–April–May (MAM), all together encompassing a total of 8 individual 3-months intervals, respectively. The EOF analysis is computed on the seasonal anomalies averaged in these 3-month bins with the reference year being the year of the last month. Thus ASO, SON and OND

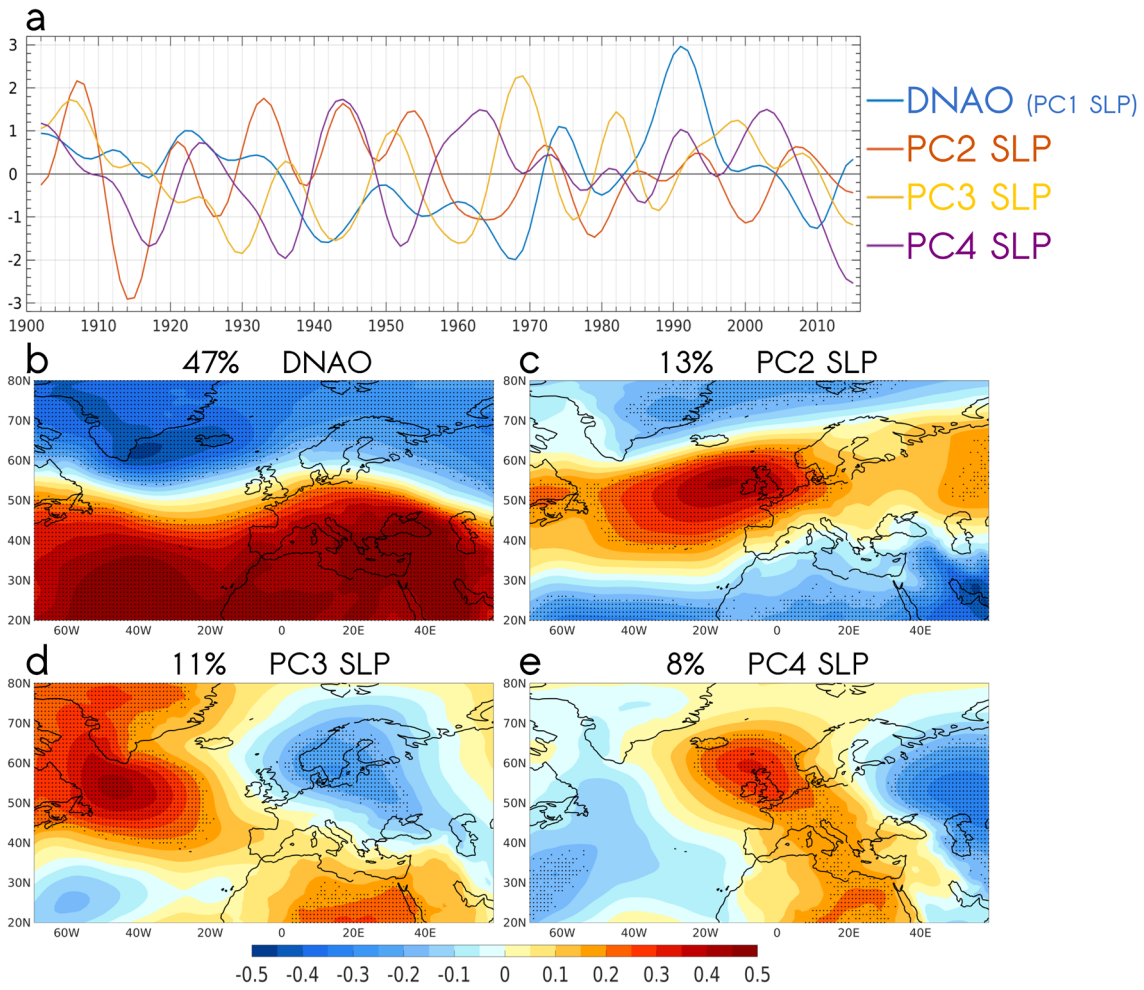

Fig. 2 Indices of decadal SLP variability (PCs) and their associated spatial patterns calculated from the leading empirical orthogonal functions (EOFs). EOF analysis is applied over low-frequency filtered (using a low-pass Butterworth filter with a 10-year cutoff period) anomalies of residual SLP over the North Atlantic-European sector (70 W–60 E, 20–80 N) (see details on calculations in Sect. 2.3). (**a**) The 1901–2015 standardized DNAO (SLP PC1) (blue line), SLP PC2 (orange line), SLP PC3 (yellow line) and SLP PC4 (purple line) time series obtained from EOF analysis applied on anomalous SLP data from NOAA-CIRES-DOE 20CRv3 reanalysis data set. **b** DNAO SLP (hPa std^{-1}) pattern calculated as the regression of anomalous residual SLP onto the DNAO index. **c** As for (**b**) but for the PC2. **d** As for (**b**) but for the PC3. (**e**) As for (**b**) but for the PC4. The percentages of explained variance from EOF analysis are 47, 13, 11 and 8% for DNAO, SLP PC2, SLP PC3 and SLP PC4 respectively

correspond to the years 1901–2014, while the remaining 3-month periods correspond to the years 1902–2015. PCP anomalies are standardized as it is common practice for variables that exhibit non-normal distributions (e.g., Comrie and Glenn 1998; Hamann and Wang 2006). The trend is not removed from individual RVs since we are interested in attributing it to a plausible external cause. Prior to EOF analysis, a Butterworth low-pass filter of order 4 with a 10-year cut-off period is applied to extract decadal and longer time scales. Note that there is no multicollinearity between individual RVs due to orthogonality between EOFs. Given the 8 possible combinations of 3-month periods (ASO, SON, OND, NDJ, DJF, JFM, FMA, MAM) and 2 fields (PCP, TEMP), we count a total of 16 case studies (RV_i^{PCP} and RV_i^{TEMP} where i = 1, 2,…, 8). The CCA is applied for each EV-RV_i combination. All individual variables (time series) within EV and RV_i are standardized prior to CCA to have unit variance.

The number of single variables (i.e., PCs) that make up each RV_i depends on the cumulative explained variance from EOF analysis on both PCP and TEMP fields, which are depicted in Table 1. The calculations involve a total of 112 EOFs with their associated PCs time series and spatial patterns (not shown). We account for seven individual variables (i.e., PC1 to PC7) within RV_i^{PCP}, which retain percentages of variance explained in PCP between 72% (SON and OND) and 79% (JFM). Note that a greater number of PCs, which therefore increases the retained explained variance in PCP,

Table 1 Cumulative explained variance in the truncated EOF space

No. of EOFs (PCs)		1	2	3	4	5	6	7
PCP	ASO	0.20	0.34	0.45	0.54	0.63	0.69	0.74*
	SON	0.18	0.31	0.44	0.53	0.60	0.66	0.72*
	OND	0.17	0.32	0.45	0.55	0.63	0.68	0.72*
	NDJ	0.23	0.39	0.51	0.60	0.65	0.71	0.76*
	DJF	0.28	0.43	0.55	0.64	0.69	0.74	0.78*
	JFM	0.28	0.43	0.53	0.61	0.69	0.74	0.79*
	FMA	0.21	0.36	0.47	0.57	0.65	0.70	0.74*
	MAM	0.18	0.34	0.46	0.55	0.63	0.69	0.74*
TEMP	ASO	0.77	0.88	0.92	0.95*	0.96	0.97	0.98
	SON	0.65	0.86	0.91	0.94*	0.96	0.97	0.98
	OND	0.55	0.85	0.90	0.94*	0.96	0.97	0.98
	NDJ	0.55	0.80	0.88	0.92*	0.95	0.96	0.97
	DJF	0.62	0.78	0.88	0.92*	0.94	0.96	0.97
	JFM	0.65	0.82	0.90	0.93*	0.95	0.97	0.98
	FMA	0.66	0.85	0.92	0.94*	0.96	0.97	0.98
	MAM	0.70	0.87	0.93	0.95*	0.97	0.98	0.99

Asterisks denote the explained variance retained by the number of EOFs (PCs) selected for CCA analysis. The number of individual components within each RV_i is determined by those values

was not found to significantly modify the results. As for RV_i^{TEMP}, four individual response variables are considered, keeping between 92% (NDJ and DJF) and 95% (ASO and MAM) of variance explained in TEMP.

4 Case studies

By construction, the maximum number of canonical modes that can be extracted from the two sets of variables equals the number of variables (columns) in the smaller matrix, EV or RV. The first pair of canonical variates (first canonical mode) is determined so as to have the highest intercorrelation between a linear combination of the EV and the corresponding linear combination of the RV. The second pair of canonical variates is then determined so that it exhibits the optimal relationship between the two sets of variables, not accounted for by the first pair of variates and so forth. Successive pairs of canonical variates are based on residual variance, and their respective canonical correlations become smaller as each additional function is extracted. Therefore, successive canonical time series (pairs of canonical variates) are orthogonal (i.e., uncorrelated) and independent of all other canonical time series derived from the same dataset. Given that the EV set contains a total of seven individual variables (DNAO, $PC2_{SLP}$, $PC3_{SLP}$, $PC4_{SLP}$, AMDV, IPO, GW), the CCA provides seven canonical modes for each PCP case study (seven PCP PCs were retained for RV_i^{PCP}) and four canonical modes for each TEMP case study (four TEMP PCs were retained for RV_i^{TEMP}). From a total of 49 canonical modes for PCP and 28 for TEMP, we explore those canonical modes for which the contribution of individual EVs, or a combination thereof (if any) is found to be significant. Given that the variance explained by successive canonical modes decreases progressively, the most consistent results according to statistical significance (see Appendix 2 for extended information) are found within the three leading canonical modes in all cases. From these leading modes, we select two sequences spanning 3-month periods for both PCP and TEMP. This selection is based on a consistent and coherent evolution of the canonical variates from ASO to MAM. These sequences of canonical PCP and TEMP variates undergo mechanistic exploration. As shown in the next section for both fields, one of the sequences exhibits oscillatory behavior in terms of decadal-to-multidecadal variability, while the remaining sequence of canonical modes depict an evident long-term trend on a secular scale with a certain oscillatory behavior.

5 Results

5.1 Long-term temperature drivers

The first sequence of canonical TEMP modes show the leading role of the GW signal expressed by high and significant values of canonical cross-loadings (Fig. 3; left column). The four leading PCs of residual SLP that represent internal atmosphere variability do not make significant contributions, although the contributions of DNAO and the SLP PC2 are comparatively high from DJF to FMA (Fig. 3m–s). Regarding the SST-forced component of TEMP, despite relatively

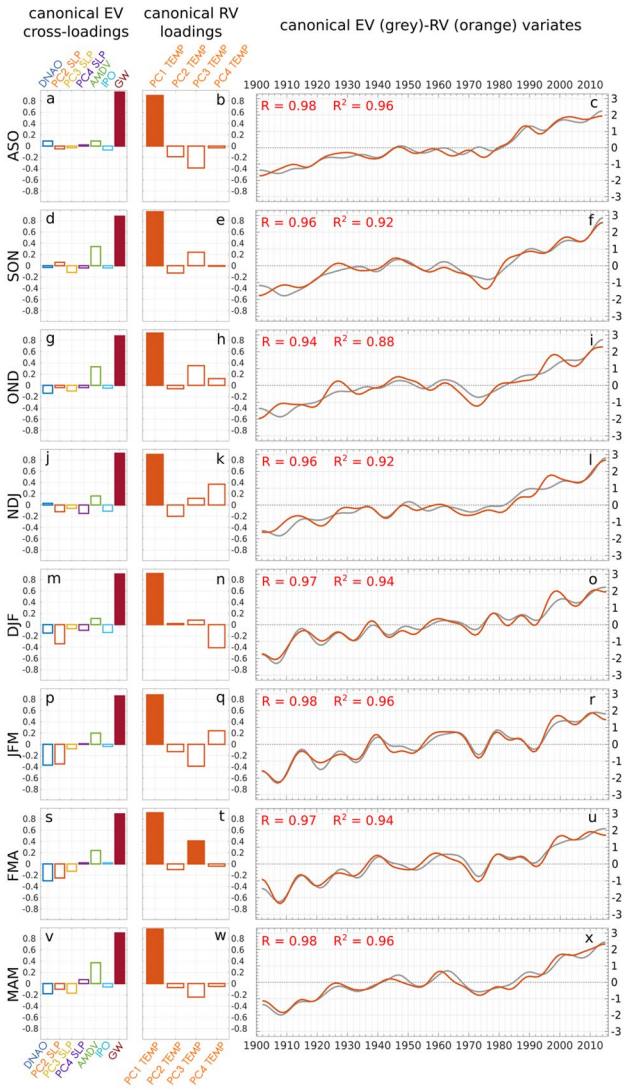

Fig. 3 First sequence of canonical TEMP modes obtained from CCA applied between the EV and RV sets. Results are shown for canonical EV cross-loadings (left column; unitless), canonical RV loadings (middle column; unitless) and pairs of canonical EV-RV variates (right column; std deviation). See Appendices 1 and 2 for detailed explanations on CCA results. Individual EVs are identified by colors: DNAO (blue), SLP PC2 (orange), SLP PC3 (yellow), SLP PC4 (purple), AMDV index (green), IPO index (turquoise) and GW index (burgundy). Individual RVs correspond to TEMP PCs from 1 to 4. Color shaded bars denote statistical significance of canonical loadings and cross-loadings at the 0.05 (95%) level under a non-parametric Ebisuzaki test. Canonical correlations (R) and their corresponding shaded variances (R^2) are indicated for significant canonical modes under objective selection criteria (see Appendix 2 for details). Canonical EV (RV) variates are depicted by grey (orange) lines. The results are shown for 3-month periods as follows: August-to-September (ASO; **a**–**c**), September-to-November (SON; **d**–**f**), October-to-December (OND; **g**–**i**), November-to-January (NDJ; **j**–**l**), December-to-February (DJF; **m**–**o**), January-to-March (JFM; **p**–**r**), February-to-April (FMA; **s**–**u**) and March-to-May (MAM; **v**–**x**)

high canonical cross-loadings associated with the AMDV for SON and OND, their values are not statistically significant (Fig. 3d–g). The TEMP response is entirely represented by the leading TEMP PCs (Fig. 3; middle column), which retain the highest percentages of TEMP variance, between 55% for OND and NDJ, and 77% for ASO. There is a significant contribution of TEMP PC3 in FMA (Fig. 3t), even though it is associated with low (7%) TEMP variance. The variances explained in TEMP by the successive EOF modes are shown in Table 1 in terms of their cumulative values. Consequently, the canonical variates exhibit a clear positive long-term trend, slightly modulated by non-significant contributions of internal atmospheric and SST-forced multidecadal variability (Fig. 3; right column). In all cases, high canonical correlations ranging from 0.94 in OND to 0.98 in ASO, JFM and MAM point out robust statistical associations likely involving real physical processes.

There is general consensus that increasing concentrations of anthropogenic GHGs are responsible for rising worldwide temperatures due to radiative forcing (e.g., Myhre et al 1998; Collins et al. 2006; Feldman et al. 2015). In line with these works, the canonical EV variates are highly dominated by the GW signal, fully explaining the variance in TEMP throughout the Mediterranean region (Fig. 4; left column), which in turn is represented by the leading TEMP PCs. The sign of the response is obtained by regression of observed TEMP anomalies onto the canonical EV variates, showing significant ubiquitous warming over the whole Mediterranean basin (Fig. 4; right column). Warming is more pronounced in the Mediterranean western half, with maximum values in North Africa and the Iberian Peninsula and secondary maxima in the Middle East. Seasonally, warming is less intense during the boreal winter months (NDJ and DJF), probably due to amplification of GHG-induced warming by land surface feedback in the fall and spring months.

6 Decadal temperature drivers

The second sequence of canonical TEMP modes depict multidecadal variability (Fig. 5). By construction, this sequence operates on residual TEMP after removing the effect of long-term trends contained within the first sequence of canonical modes, and therefore it can be assumed to represent natural TEMP variability. Robust canonical modes extend from SON through JFM expressed by significant canonical correlations of 0.76, 0.81, 0.91, 0.93 and 0.87 for SON, OND, NDJ, DJF and JFM respectively. On the contrary, the canonical modes for ASO, FMA and MAM (see Fig. S1) are discarded as they do not meet one or more selection criteria exposed in Appendix 2. Relevant contributions to canonical EV variates are attributed to DNAO and AMDV from SON (Fig. 5a) to JFM (Fig. 5j) in terms

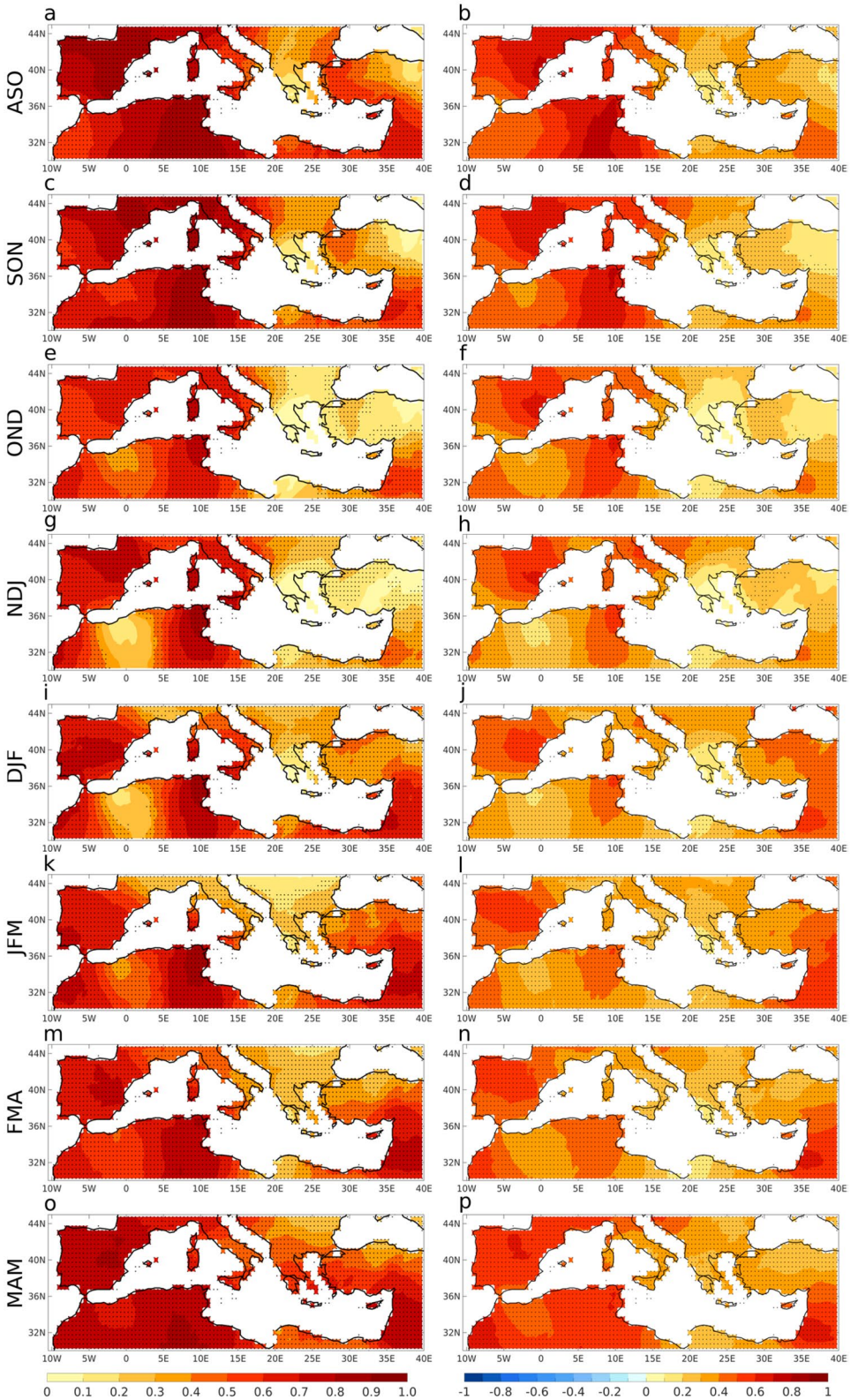

Fig. 4 Explained variance (unitless) in TEMP by the canonical EV variates at each grid point (left column) and spatial patterns of TEMP (K std^{-1}) obtained by regression of TEMP onto the canonical EV variates (right column). Results are shown over the Mediterranean (10 W–45 E, 30–45 N) study region. Stippling denotes statistical significance at the 0.05 (95%) level by applying non-parametric Monte Carlo testing. The results correspond to the first sequence of significant canonical TEMP modes and are displayed for 3-month periods as follows: ASO (**a**–**b**), SON (**c**–**d**), OND (**e**–**f**), NDJ (**g**–**h**), DJF (**i**–**j**), JFM (**k**–**l**), FMA (**m**–**n**) and MAM (**o**–**p**)

of significant canonical EV cross-loadings. The significant DNAO input remains in JFM while the AMDV contribution vanishes (Fig. 5m). Significant TEMP responses from SON to DJF are led by the second TEMP PCs (Fig. 5; middle column), the third PCs being also significant for SON and DJF (Fig. 5b–k). As for JFM, TEMP RVs are dominated by

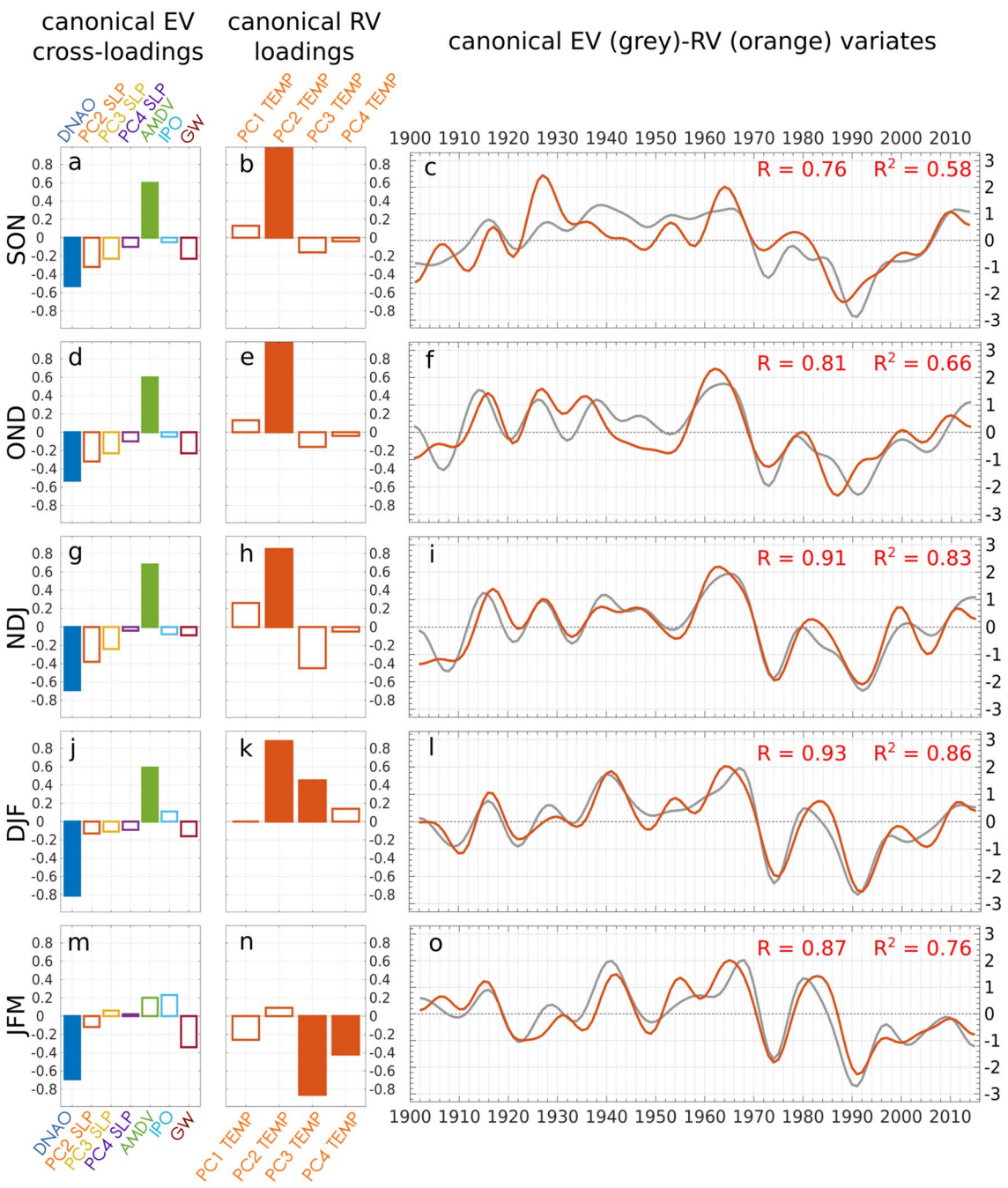

Fig. 5 The same as Fig. 3 but for the second sequence of canonical TEMP modes. The results are shown for significant canonical TEMP modes in terms of seasonal means for 3-month periods as follows: SON (**a**–**c**), OND (**d**–**f**), NDJ (**g**–**i**), DJF (**j**–**l**) and JMF (**m**–**o**)

significant contributions of PC3 and PC4 (Fig. 5n) (Percentages of explained TEMP variance associated with each PC are displayed in Table 1 expressed by cumulative values). The resulting canonical EV and RV variates (Fig. 5; right column) depict oscillatory behaviors from SON to DJF (Fig. 5c–l), with a marked negative trend from the 70 s to a minimum by 1990, followed by an upward trend (Fig. 5i–o). The behavior is the same for JFM, but the positive trend in recent decades is attenuated. The variance explained in observed TEMP anomalies by the canonical EV variates shows significant signals over the eastern Mediterranean region for SON, OND and NDJ (Fig. 6a–e), weakening for DJF and vanishing for JFM as the signal becomes significant in the northern part of the study region (Fig. 6g–i). The regression of TEMP anomalies onto the canonical EV variates denotes a zonal dipole of significant anomalies with

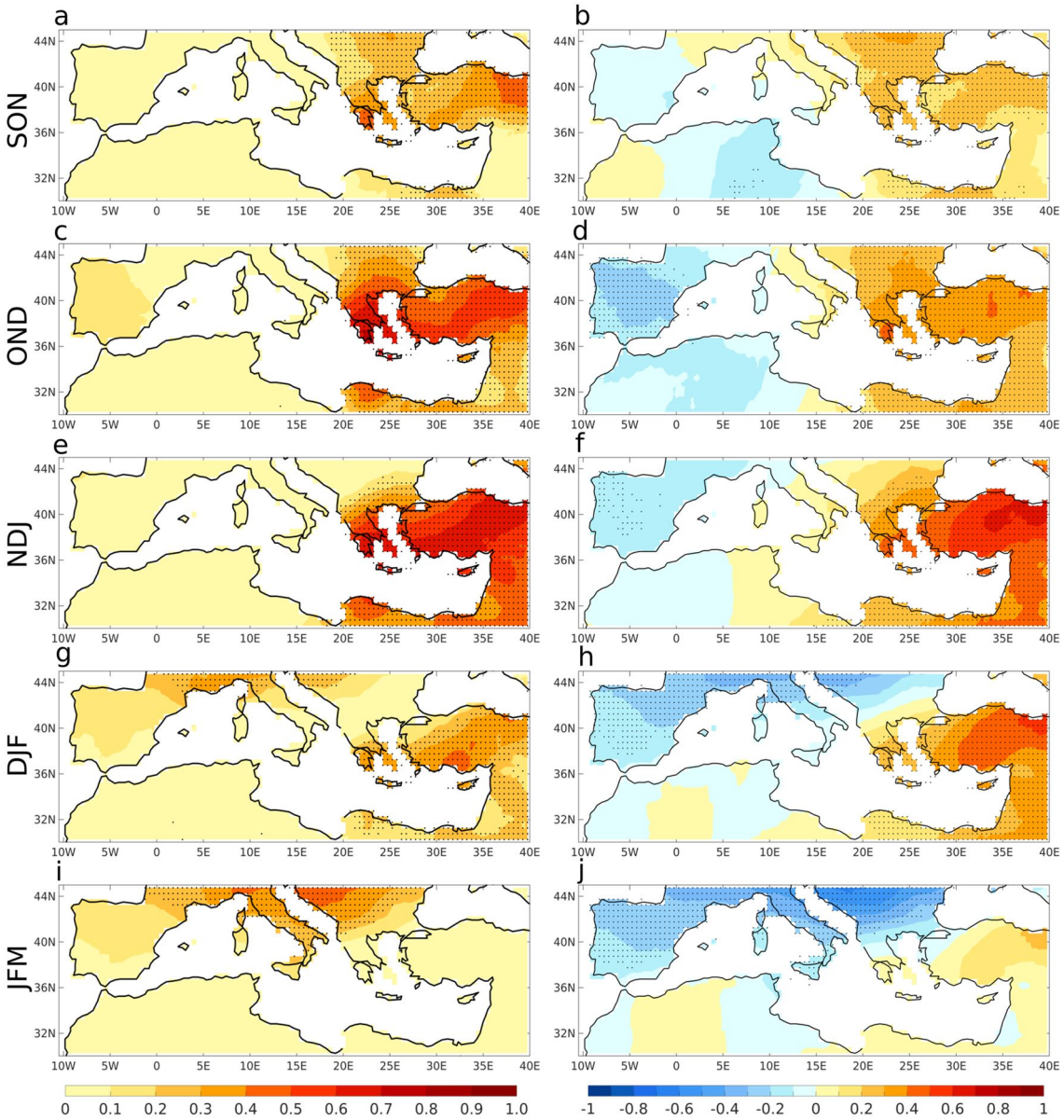

Fig. 6 The same as Fig. 4 but for the second sequence of canonical TEMP modes. The results are shown as seasonal means for 3-month periods as follows: SON (**a**–**b**), OND (**c**–**d**), NDJ (**e**–**f**), DJF (**g**–**h**) and JMF (**i**–**j**)

positive (negative) values to the east (west) for SON, OND and NDJ (Fig. 6b–f), the amplitude of the positive signal weakening in the east for DJF and JFM as negative anomalies spread eastward (Fig. 6h–j).

To explore the SST and SLP patterns associated with the second sequence of canonical modes, we regress the observed anomalies of both fields onto the canonical EV variates (Fig. 7; left and right columns respectively). The resulting SSTA maps resemble the SST pattern corresponding to the AMDV time series (cf. Fig. 1b–c), in cases for which significant contributions of AMDV were found within the EV set (SON to DJF; Fig. 7a–g). The North Atlantic Ocean pattern exhibits a SST tripole in JFM (Fig. 7i) that resembles the positive phase of the North Atlantic SST Tripole (NAT), which has been singled out as the NAO-forced response of North Atlantic SST via atmospheric forcing, primarily by surface heat fluxes and Ekamn currents (Seager et al. 2000; Czaja et al. 2003; Visbeck et al. 2003; Sun et al. 2015). Indeed, we attribute this positive NAT-like pattern to the preponderant contribution of negative DNAO in JFM (see Fig. 5m). Consistently, the regression onto anomalous SLP displays a meridional SLP dipole pattern akin to the DNAO structure over the North Atlantic-Europe-Mediterranean sector as the winter peak season approaches (Fig. 7; right

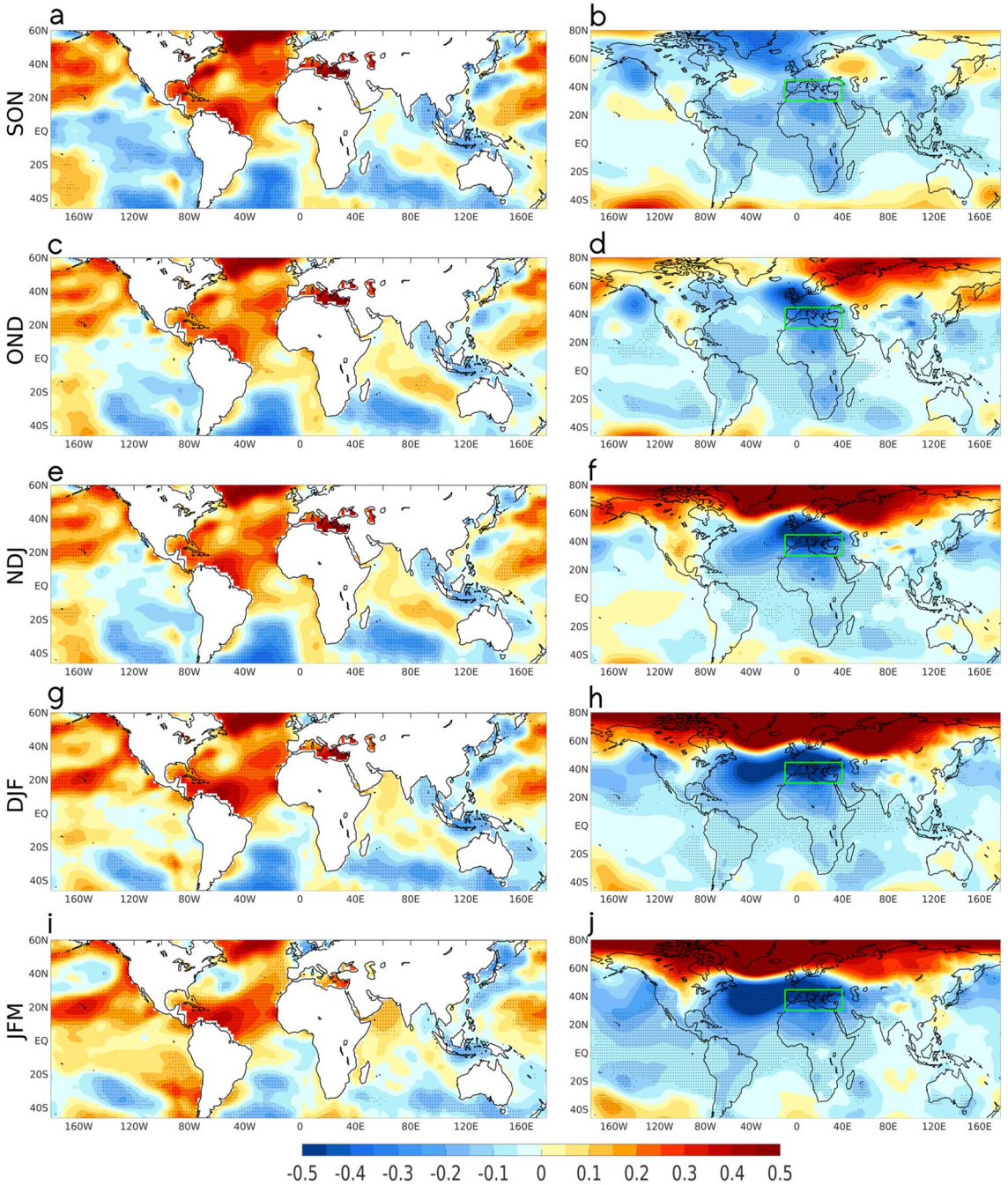

Fig. 7 Spatial patterns obtained by regression of canonical EV variates for the second sequence of canonical TEMP modes. (left column) Regression onto anomalous SST (K std^{-1}). (right column) Regression onto anomalous SLP (hPa std^{-1}). A green contour box indicates the Mediterranean (10 W–45E, 30–45 N) study region. Stippling denotes statistical significance at the 0.05 (95%) level under the Monte Carlo method. The results are shown as seasonal means for 3-month periods: SON (**a**–**b**), OND (**c**–**d**), NDJ (**e**–**f**), DJF (**g**–**h**) and JMF (**i**–**j**)

column). These SST-SLP associations show an increasing (decreasing) DNAO (AMDV) influence on TEMP variability as time evolves from fall to winter, representing the optimal ocean–atmosphere state to influence the multidecadal TEMP response over the Mediterranean study region.

To examine the physical mechanisms behind the associations between the TEMP responses and the SST-SLP patterns, we first explore the anomalous low-level atmospheric thickness associated with the canonical EV variates (Fig. 8; left column). The intra-seasonal variation of the anomalous

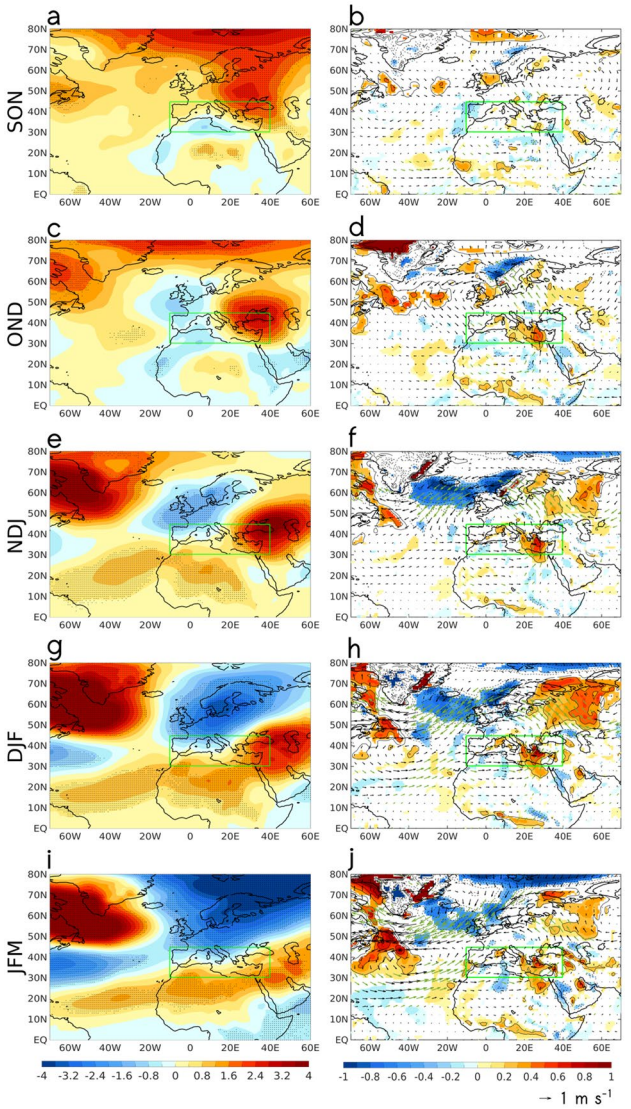

Fig. 8 Spatial patterns obtained by regression of canonical EV variates for the second sequence of canonical TEMP modes. (left column) Regression onto anomalous low-level atmospheric thickness (m std^{-1}). Stippling denotes statistical significance at the 0.05 (95%) level. (right column) Regression onto vertically integrated thermal advection (10^{-3} K Kg m^{-2} s^{-1} std^{-1}) and regression onto horizontal wind components (m s^{-1} std^{-1}) at the 850 hPa reference level. Only significant values are shown for thermal advection at the 0.05 (95%) level. Green arrows denote significant wind at the same 95% level. See Sect. 2.1 for details about calculations. Statistical significance is evaluated under the Monte Carlo method. A green contour box indicates the Mediterranean (10 W–45E, 30–45 N) study region. The results are shown as seasonal means for 3-month periods: SON (**a**–**b**), OND (**c**–**d**), NDJ (**e**–**f**), DJF (**g**–**h**) and JMF (**i**–**j**)

low-level atmospheric thickness is consistent with the evolution of TEMP anomalies in a way that low-level tropospheric expansions (shrinkages) closely matches positive (negative) TEMP anomalies (cf. Fig. 6; right column), indicating air warming (cooling) in the lower troposphere. The large-scale anomalous atmospheric circulation responds to the development phase of the low-pressure system over southern Europe in SON and OND (Fig. 7b–d), which later establishes over the Mediterranean basin to form the low pressure lobe relative to the negative DNAO phase (Fig. 7f–j). At the same time, positive TEMP anomalies in the Middle East dissipate (see Fig. 6f–j), coinciding with the weakening of the Mediterranean SST warming (see Fig. 7e–i). The low-pressure system drives an advective warming of the East Mediterranean/Middle East associated with southerly flow that advects warm air into this region (Fig. 8; right column). As the season progresses, the flow becomes south westerly and even westerly, stretching the region fed by warm advection eastward, in a zonal direction, where the largest anomalies in TEMP occur (cf. Fig. 6; right column). Over the east Atlantic and Western Europe, the cold anomaly is associated with advection by northeasterly winds driven by the same low-pressure system.

6.1 Decadal precipitation drivers

The first sequence of canonical PCP modes depicts decadal-type oscillatory behavior (Fig. 9). Analogous to the case of decadal TEMP variability (see Sect. 3.2), significant contributions to PCP variability are attributed to the combined effect of DNAO and AMDV from OND to FMA (Fig. 9; left column), with the DNAO being the only significant input in the winter peak season (DJF; Fig. 9m). The response signal (i.e., canonical EV variate) is obtained as a combination of DNAO and AMDV in their opposite phases (i.e., opposite signs of their associated canonical cross-loadings in Fig. 9; left column). Significant high canonical correlations of 0.97 from NDJ to FMA highlight robust associations and likely physical realism. The relation is weaker in OND ($R = 0.72$), but consistent in terms of the significant DNAO and AMDV influence. The canonical RV variates are represented by the leading PCs of PCP from OND to JFM (Fig. 9; middle column), with a significant input of PC5 in OND, although it only retains 8% of variance explained in PCP. In FMA, the PCP response is represented by the second PCP PC (Fig. 9n). Regarding the remaining 3-month seasons (ASO, SON, MAM), their corresponding CCA-related results are discarded for further exploration due to unfulfilled selection criteria (see Fig. S2).

To infer a causality link, we first examine the variance explained in observed PCP anomalies by the canonical EV variates (Fig. 10; left column). The resulting patterns evolve from fall into consistent, widespread signals in DJF and JFM (Fig. 10e–g) with maxima over Iberia, Italy, the Balkans and Turkey. The sign of the response is determined by regression of the observed PCP anomalies onto the canonical EV variates (Fig. 10; right column). In the winter peak season (DJF), significant positive anomalies are observed

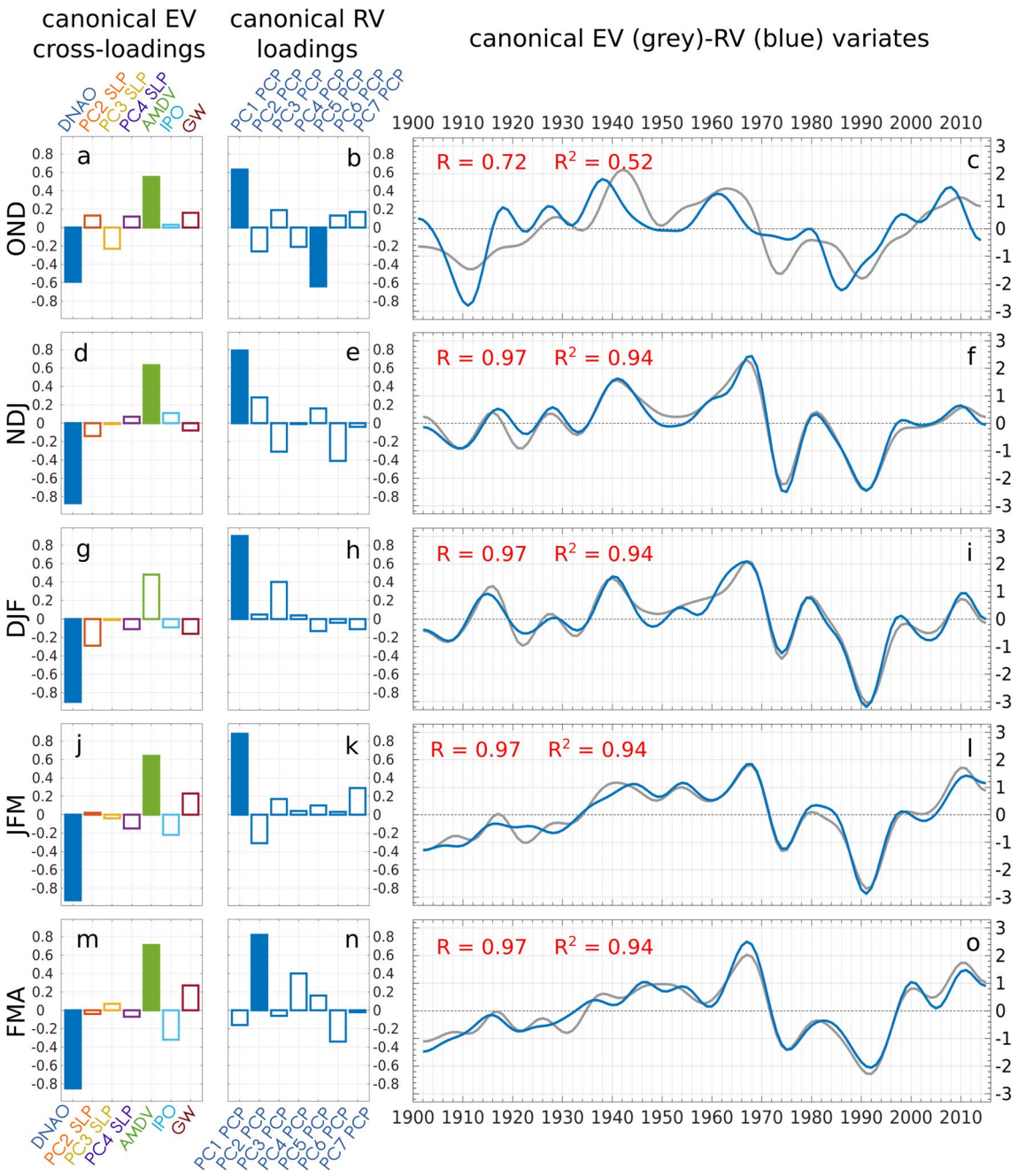

Fig. 9 The same as Fig. 3 but for the first sequence of canonical PCP modes. The results are shown for significant canonical PCP modes (see Appendix 2 for details) and are displayed for 3-month periods as follows: OND (**a–c**), NDJ (**d–f**), DJF (**g–i**), JFM (**j–l**) and FMA (**m–o**)

in the Iberian Peninsula, Morocco, Italy, Balkan Peninsula, Turkey and Syria and negative anomalies in Tunisia, Israel and the coasts of Libya and Egypt (Fig. 10f). This quasi-meridional PCP dipole occurs in response to the dominant influence of the DNAO in DJF (Fig. 9m). Positive scores of the projected index predominate until the end of the 60 s, followed by a phase change with pronounced negative values in the 90 s and an apparent positive trend in the recent decades (Fig. 9o). Transitions to and from DJF are associated with significant contributions of AMDV in combination with DNAO, following an evolution consistent with the PCP pattern described above. Notably, drying spreads in North Africa and northward through Italy in JFM and FMA (Fig. 10h–j).

The SST and SLP patterns associated with the canonical modes are obtained by regression of both anomalous fields onto the canonical EV variates (Fig. 11; left and right columns respectively). The SST patterns are reminiscent

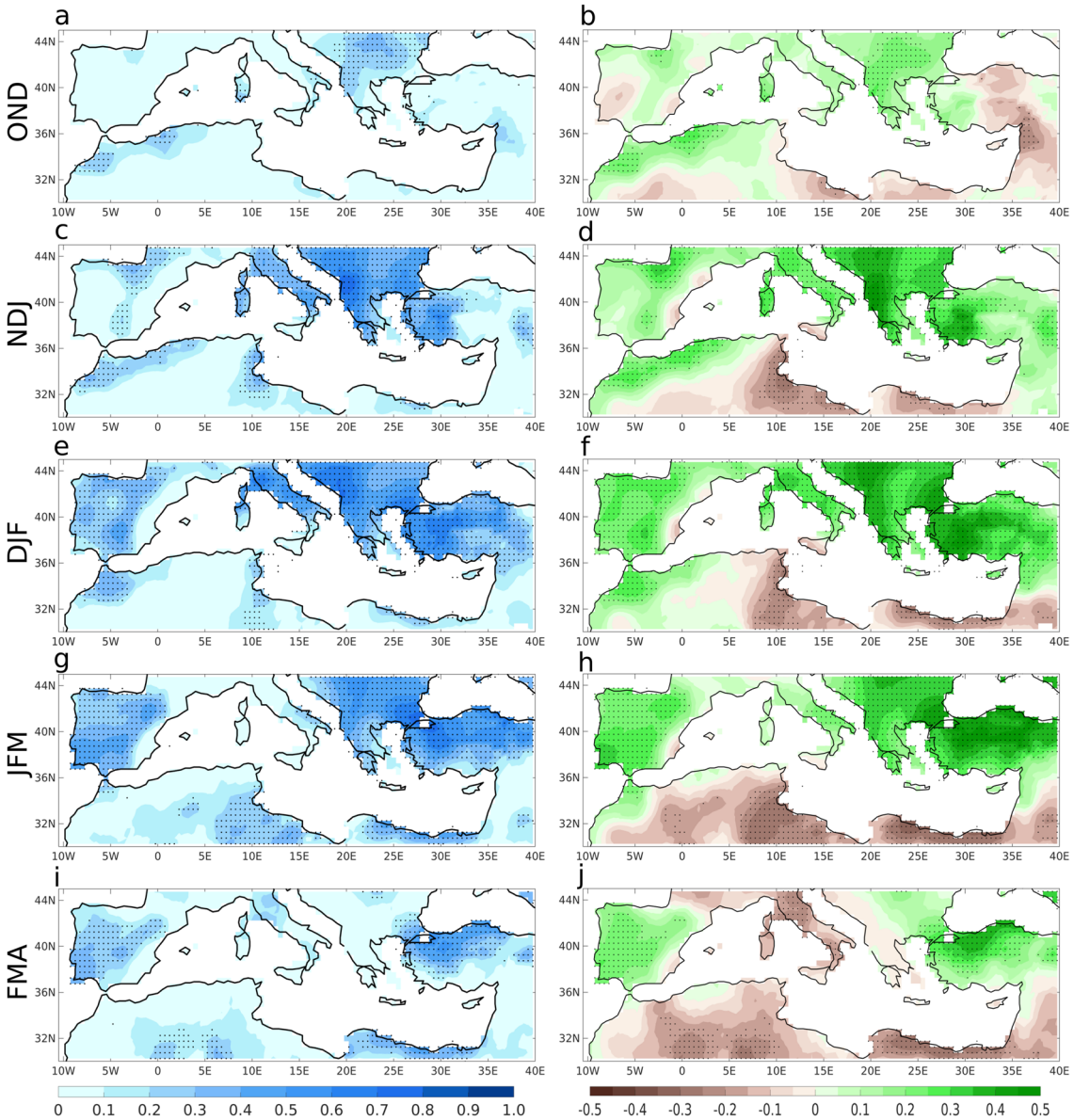

Fig. 10 Explained variance (unitless) in PCP by the canonical EV variates at each grid point (left column) and spatial patterns of PCP (mm day^{-1} std^{-1}) obtained by regression of PCP onto the canonical EV variates (right column). Results are shown over the Mediterranean (10 W–45E, 30–45 N) study region. Stippling denotes statistical significance at the 0.05 (95%) level by applying non-parametric Monte Carlo testing. The results are shown for the first sequence of significant canonical TEMP modes and are displayed for 3-month periods as follows: OND (**a**–**b**), NDJ (**c**–**d**), DJF (**e**–**f**), JFM (**g**–**h**) and FMA (**i**–**j**)

of AMDV (cf., Fig. 1b–c), and a SSTA tripole pattern in DJF (Fig. 11e) that resembles the ocean response to the negative phase of DNAO (e.g., Cayan 1992; Visbeck et al. 2003), consistent with the dominant contribution of DNAO in the winter peak season (see Fig. 9g). Indeed, the accompanying SLP pattern (Fig. 11f) resembles the negative DNAO phase (cf. Fig. 2b) and this SLP structure is also present earlier in NDJ and later in JFM (Fig. 11d–h) but not in OND and FMA (Fig. 11b–j).

The prominent contributions of AMDV and DNAO can be interpreted as the optimal ocean–atmosphere state to drive multidecadal PCP variability in the Mediterranean basin. In this context, DNAO is assumed as the leading driver, prevailing during the winter peak seasons (NDJ to JFM), whereas in the autumn-to-winter (OND) and winter-to-spring (FMA) transitions the AMDV acts to partially compensate for DNAO development and decline phases respectively. The low-pressure system centered over the

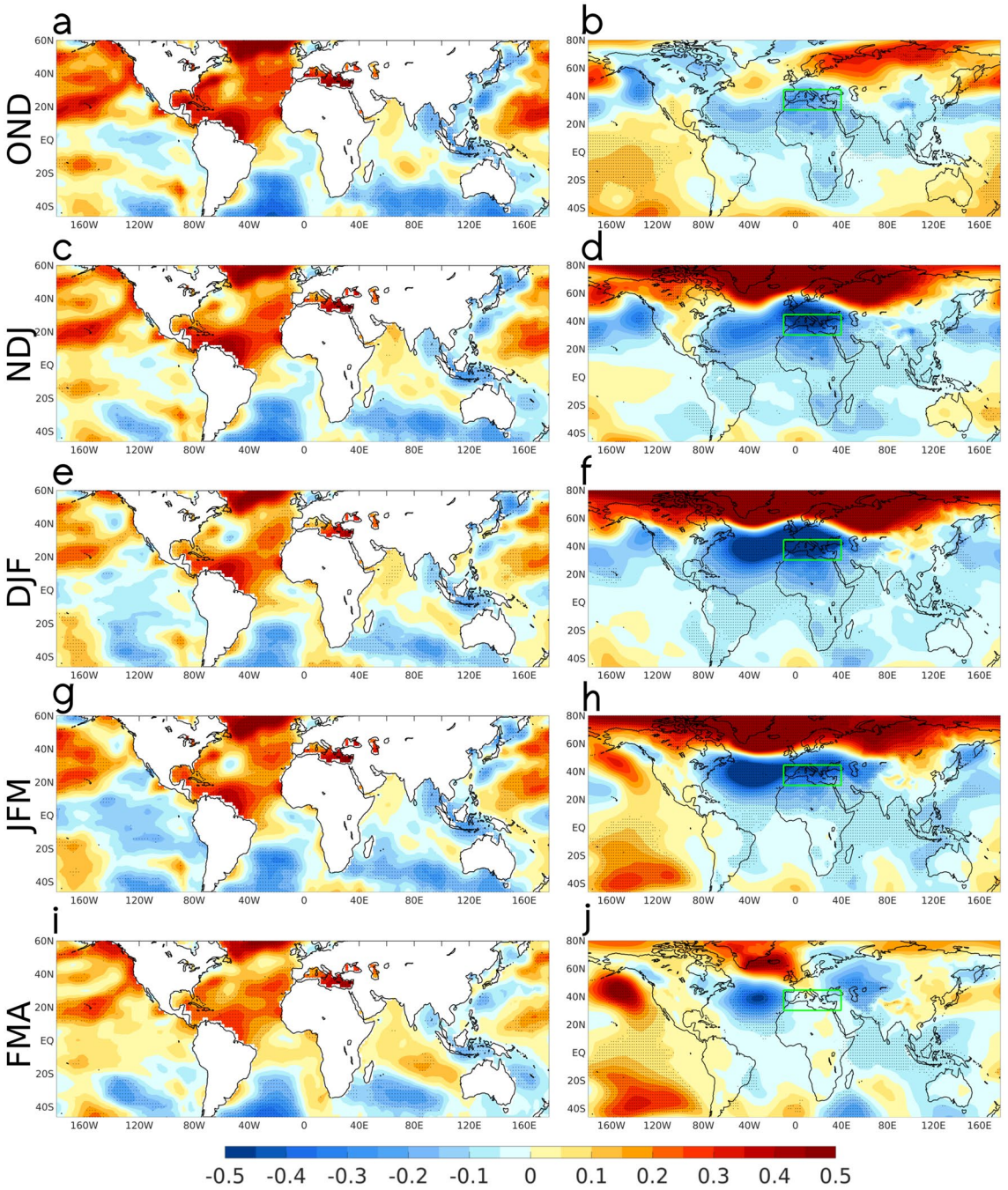

Fig. 11 Spatial patterns obtained by regression of canonical EV variates for the first sequence of canonical PCP modes. (left column) Regression onto SSTA (K std^{-1}). (right column) Regression onto SLP anomalies (hPa std^{-1}). A green contour box indicates the Mediterranean (10 W–45E, 30–45 N) study region. The results are shown for the first sequence of significant canonical PCP modes and are displayed for 3-month periods as follows: OND (**a**–**b**), NDJ (**c**–**d**), DJF (**e**–**f**), JFM (**g**–**h**) and FMA (**i**–**j**)

Mediterranean region and mid-latitude area of the North Atlantic, which is associated with the negative DNAO phase, enhances moisture transport to the Mediterranean basin (Fig. 12; left column). This low-level moisture input feeds convergence across the Mediterranean basin, being consistent with the PCP responses shown in Fig. 10 (right column), which are more intense under stronger DNAO activity in the winter peak season. In the winter-to-spring transition (FMA), the changing PCP response is related to the decay of DNAO, with weaker convergence over the Mediterranean region (Figs. 11j, 12m), but positive PCP anomalies in the Iberian Peninsula and Turkey, while drying spreads north

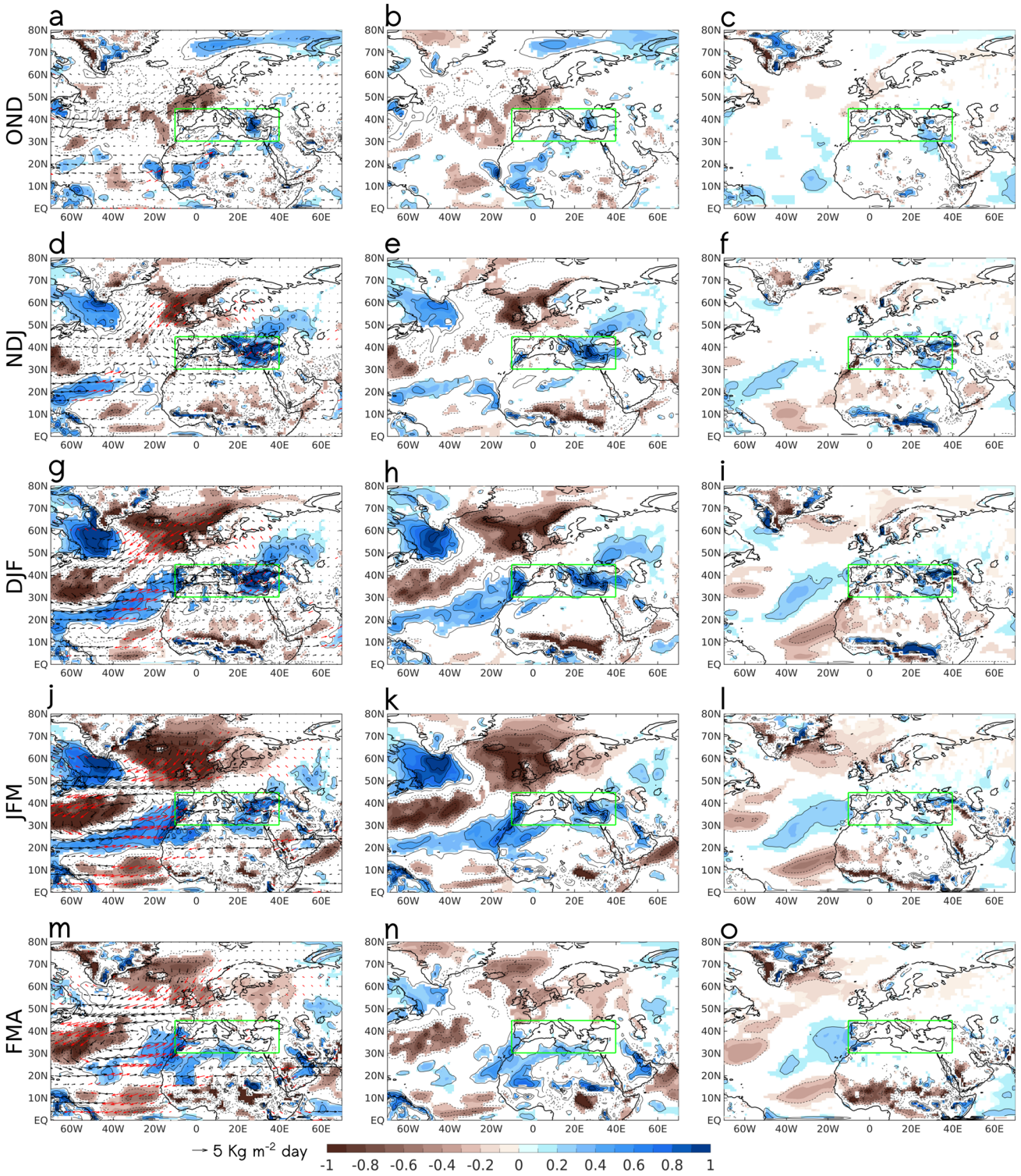

Fig. 12 Spatial patterns obtained by regression of canonical EV variates for the first sequence of canonical PCP modes. (left column) Regression onto vertically integrated MFC (10^{-1} kg m^{-2} day^{-1} std^{-1}; shaded) and regression onto vertically integrated moisture transport (Kg m^{-1} day^{-1} std^{-1}; arrows). (middle column) Regression onto vertically integrated advection term of MFC (10^{-1} kg m^{-2} day^{-1} std^{-1}). (right column) Regression onto vertically integrated convergence term of MFC (10^{-1} kg m^{-2} day^{-1} std^{-1}). See Sect. 2.1 for details about calculations. Only significant values are shown at the 0.05 (95%) level. Green arrows denote significant wind at the same 95% level. Statistical significance is assessed under the Monte Carlo method. A green contour box denotes the Mediterranean (10 W-45 E, 30–45 N) study region. The results are shown as seasonal means for 3-month periods: OND (**a**–**c**), NDJ (**d**–**f**), DJF (**g**–**i**), JFM (**j**–**l**) and FMA (**m**–**o**)

through Italy (Fig. 10j). Additional calculation of the advection and convergence terms of MFC (Fig. 12; middle and right columns respectively) shows that significant anomalies of both components are relevant to the full MFC, and that the moisture advection anomaly is potentially associated with AMDV-related SST anomalies in the North Atlantic basin and Mediterranean Sea.

6.2 Long-term precipitation drivers

The second sequence of canonical PCP modes is characterized by multidecadal variability signals with marked positive long-term trends (Fig. 13). High significant canonical correlations, between 0.81 and 0.92, underlie the canonical modes from OND (Fig. 13g–i) to MAM (Fig. 13v–x). The leading significant contributions within the EV set are attributed in all cases to the GW signal (Fig. 13; left column), with secondary inputs of SLP PC4 in JFM (Fig. 13j), and SLP PC2 in FMA (Fig. 13m). The PCP responses are represented by diverse PCP PCs (Fig. 13; middle column), with the leading PC playing only a significant role in MAM (Fig. 13q). Depending on the 3-month period being analyzed, the variance explained in PCP by the canonical EV variates shows significant signals in the southeastern Mediterranean region, North Africa, the Iberian Peninsula, Greece and western Balkans (Fig. 14; left column). The PCP patterns associated with the canonical modes depict negative, widespread anomalies (Fig. 14; right column). Notable exceptions include positive PCP anomalies in the Balkan Peninsula in DJF (Fig. 14f) and a small region of Algeria in FMA (Fig. 14j). As for ASO and SON, their corresponding CCA modes are not consistent enough (see Fig. S3).

Given the projected widening and weakening of the Hadley circulation under GW (e.g., Gastineau et al. 2008; Hu et al. 2013; Tao et al. 2016; Grise et al. 2019), we consider whether decreased PCP in the Mediterranean basin could be a response to the northward shift of the subtropical dry zone, and use the Hadley cell metric based on the meridional mass stream function to explore anomalies of the Hadley circulation. Since the canonical EV variates are dominated by the GW signal, their regression onto anomalous meridional mass stream function is also interpreted as the GW-induced anomalous mean meridional circulation (Fig. 15; left column). We do not see a northward displacement of the descending branch of the Hadley circulation (compare the anomalous and climatological stream functions in Fig. 16) but do see a weakening of the downward mass flux in NDJ, DJF, JFM and FMA (Fig. 15c–i). The decreased PCP as shown in Fig. 14 (right column) is therefore not explained by a poleward shift of the subtropical dry zone, a result which is, however, consistent with anthropogenic tropical expansion in the northern hemisphere being weaker than in the southern hemisphere and so far difficult to identify under a background of large natural variability (e.g., Grise et al. 2019). Nevertheless, this calculation refers to the zonal mean Hadley Cell and does not disqualify a hypothetical local incursion of the subtropical dry zone into the Mediterranean region. Indeed, regression onto anomalous SLP does reflect a northward shift of the high-pressure system over North Africa into the Mediterranean basin (Fig. 15; right column). This atmospheric configuration is consistent with a local poleward expansion of the subtropical subsidence region inducing a drying trend and negative PCP anomalies. Consistently, lobes of positive PCP anomalies are observed in regions where the positive SLP is not significant, as is the case of the Balkan Peninsula in DJF (Fig. 14f, 15f) and FMA (Fig. 14j, 15j).

7 Conclusions and discussion

7.1 Conclusions

We carried out a statistical analysis of the historical observations using a CCA-based method applied to the combined, multi-component matrix representing several, known large-scale drivers of PCP and TEMP in the Mediterranean region during the half-year wet season. In this context, we separated the relative contributions of the natural, internal ocean–atmosphere variability and external anthropogenic forcing, and evaluated their respective roles in driving decadal and longer-term Mediterranean hydroclimate variability. The following conclusions have been reached:

- Decadal-to-multidecadal PCP and TEMP variability are associated with dominant contributions of AMDV and DNAO. These contributions, expressed as linear combinations of their respective time series, are interpreted as optimal ocean–atmosphere configurations that cause effective PCP and TEMP responses. In this context, we note that the relevant role of Atlantic-Mediterranean SST variability during the winter season has been overlooked so far. In all cases, the DNAO appears as the leading thermal and hydroclimate driver, as it is the dominant (unique) contribution in the winter peak season (TEMP in JFM and PCP in DJF), while AMDV acts to enhance these responses. DNAO in its negative phase and AMDV in its positive phase (as defined here) act together in a way that during winter they enhance moisture and heat transport from the warmer North Atlantic Ocean inland, and locally from the warmer Mediterranean Sea towards the northern rim of the Basin. The secondary role of AMDV is more relevant in the fall-to-winter and winter-to-spring transitions, when the DNAO pattern is not dominant.

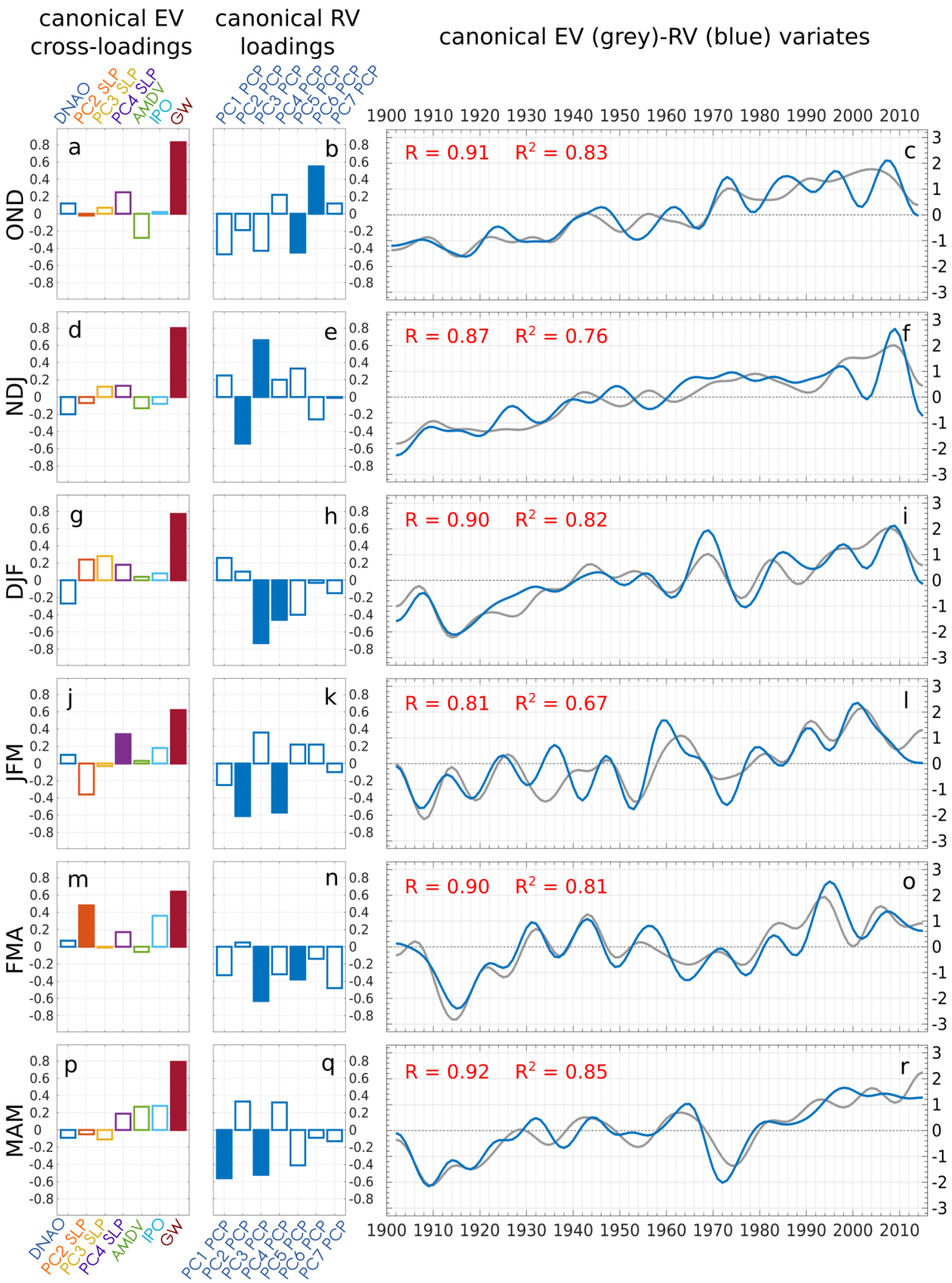

Fig. 13 The same as Fig. 3 but for the second sequence of canonical PCP modes. The results are shown for significant canonical PCP modes in terms of seasonal means for 3-month periods as follows: OND (**a**–**c**), NDJ (**d**–**f**), DJF (**g**–**i**), JMF (**j**–**l**), FMA (**m**–**o**) and MAM (**p**–**r**)

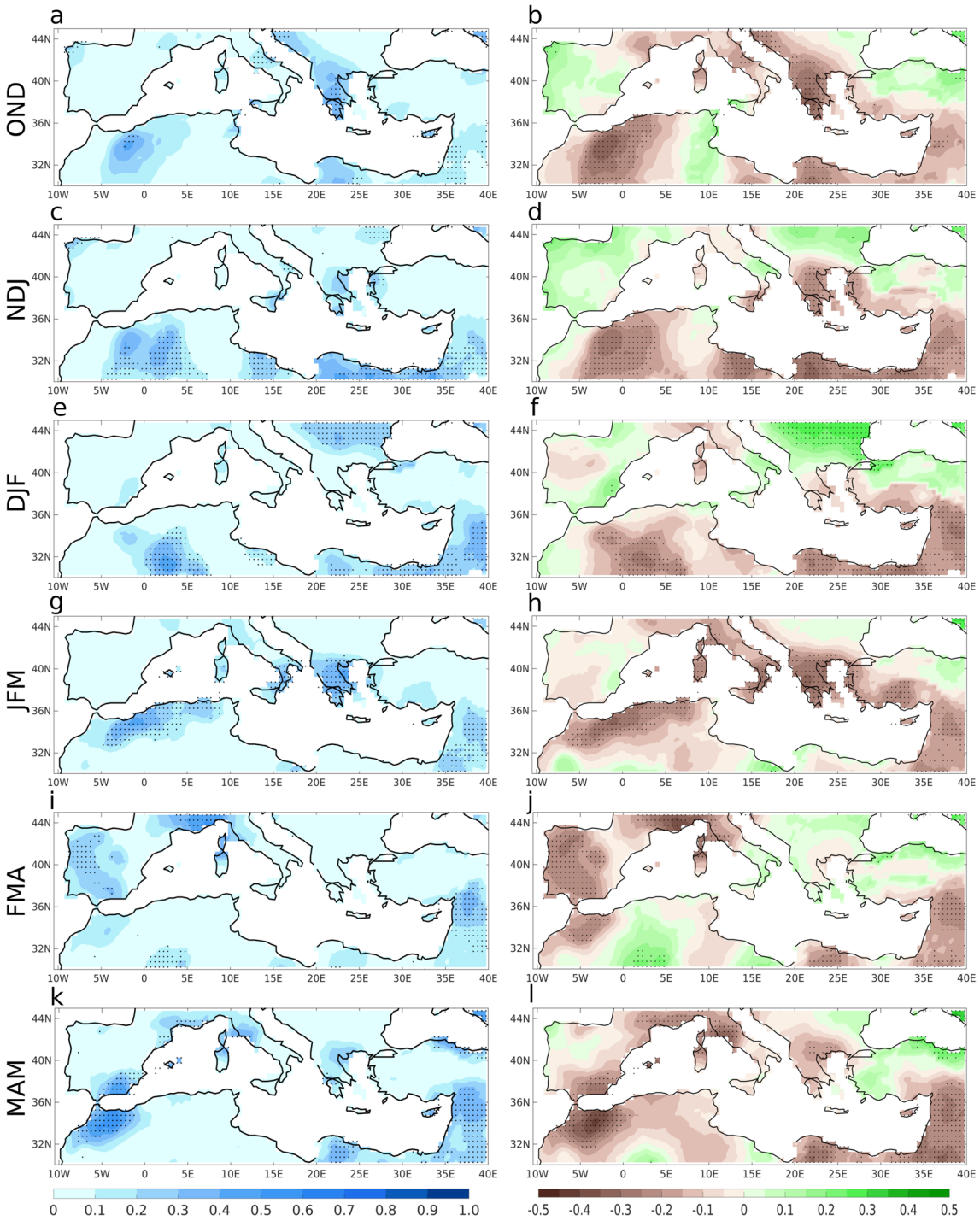

Fig. 14 The same as Fig. 11 but for the second sequence of canonical PCP modes. The results are shown as seasonal means for 3-month periods as follows: OND (**a**–**b**), NDJ (**c**–**d**), DJF (**e**–**f**), JMF (**g**–**h**), FMA (**i**–**j**) and MAM (**k**–**l**)

- We corroborate the widespread TEMP increase in response to anthropogenic radiative forcing (Lashof and Ahuja 1990; Myhre et al 1998; Jain et al. 2000; Collins et al. 2006; Scheutz et al. 2009; Feldman et al. 2015). This anthropogenic warming combines with the naturally forced dipole of decadal TEMP anomalies. Consequently, the merged effect of DNAO with AMDV in their negative and positive phases respectively, dampen the warming in the western Mediterranean, while exacerbating it in the eastern half and vice versa for a phase reversal of DNAO and AMDV. Chronologically, in the decades prior to the 1970s, the decadal variability of TEMP was dominated

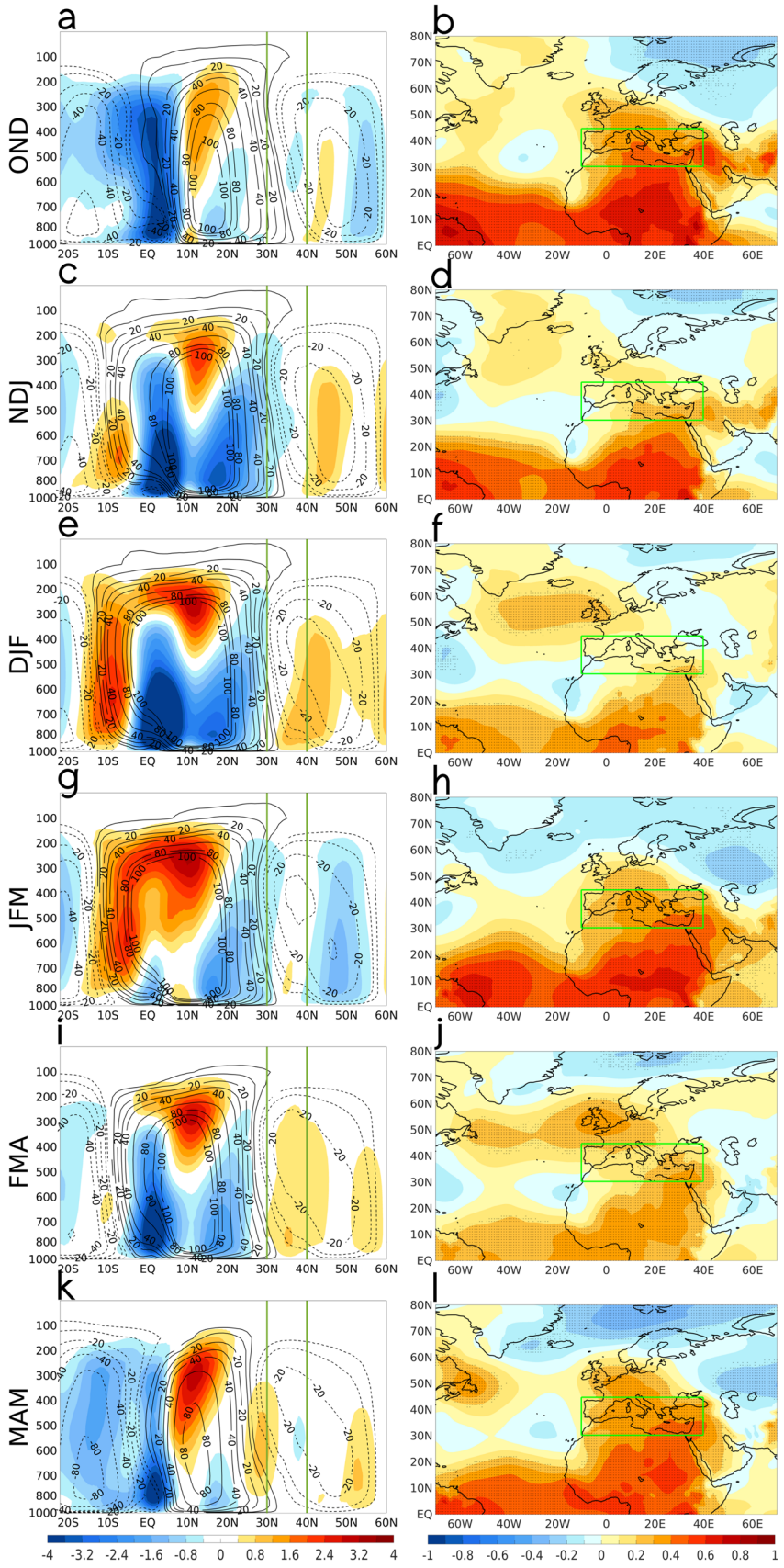

Fig. 15 Spatial patterns obtained by regression of canonical EV variates for the second sequence of significant canonical PCP modes. (left column) Regression onto anomalous stream function (shaded; 10^9 kg s^{-1}). Only significant values are shown at the 0.05 (95%) level. Zonal mean mass streamfunction is indicated by contours with positive values (solid lines) and negative values (dashed lines) indicating clockwise and counterclockwise mass flux respectively. (right column) Regression onto SLP anomalies (hPa std^{-1}). Stippling denotes statistical significance at the 0.05 (95%) level. Statistical significance is assessed under the Monte Carlo method. Green vertical lines delimit the southern and northern edges (30–45 N) of the Mediterranean study region. The results are shown for 3-month periods as follows: OND (**a**–**b**), NDJ (**c**–**d**), DJF (**e**–**f**), JMF (**g**–**h**), FMA (**i**–**j**) and MAM (**k**–**l**)

by natural forcing. Thus, in the early twentieth century, negative AMDV conditions, together with the positive DNAO phase, promoted warmer TEMP in the western and northwestern Mediterranean countries, and colder temperatures than normal in the remaining Mediterranean area. In the following decades, due to the reversal of the AMDV and DNAO phases (change to their positive and negative phases respectively), the TEMP anomaly pattern was consequently reversed, so that warmer than normal conditions dominated Anatolia and the Mediterranean Middle East, as well as the Balkan Peninsula in the first months of the winter half-year season. From the 1970s until the end of the twentieth century, when anthropogenic radiative forcing became more prevalent, a new change in the phases of DNAO (positive) and AMDV (negative), exacerbated anthropogenic warming in the northwestern half of the Mediterranean basin, while alleviating it over the eastern area. In the midst of pronounced anthropogenic warming of recent decades, the trend toward positive AMDV conditions, coupled with the opposite phase of DNAO, point to excessive winter warming in the Balkan Peninsula, Anatolia, and the Middle East, while natural forcing may not be sufficient to alleviate the marked anthropogenic warming over western North Africa, the Iberian Peninsula, southern France and Italy.

- Regarding PCP, our results showed a drying trend in response to GW, which is in accordance with the projected aridification of the Mediterranean region in response to rising GHGs (Seager et al. 2019), even though the possible mechanisms underlying this drying trend are complex and difficult to identify in a context of marked natural variability. In this framework, and consistent with previous studies (e.g., Seager et al. 2014; Zappa et al. 2015), we propose that a local northward shift of the subtropical dry zone over the Mediterranean basin is in process. How this plausible local expansion of subtropical subsidence dynamically develops is worthy of future investigation, including the role of changes in stationary wave dynamics (Simpson et al. 2016).

8 Discussion

In order to develop a mechanistic understanding of robust statistical links we have focused on the 1901–2015 (114 years) period for which dynamical fields and observations are commonly available. In this framework, the relative shortness of the observational data records compared to the requirements of decadal variability analyses is a limitation in observation-based studies (e.g., for the AMV about 120 years of data are necessary to capture two full cycles). Consequently, we encourage proper application of high resolution paleoclimate proxies, such as tree rings and lake and ocean sediments. Further work based on multiple and improved data sources, and model experiments will also be necessary to corroborate the results presented herein.

Regarding the methodology, as a regression-based statistical technique applied in the context of climate variability, multivariate associations derived from CCA do not directly imply causality, even though high significant values suggest potential physical links worthy of being further explored. Likewise, canonical correlations refer to the explained variance in the canonical variates, not the original variables. Given these conditions, we explored the associations between the canonical modes and the observed anomalies of PCP and TEMP in terms of the variance explained in such anomalous fields by the canonical EV variates, which in turn were regressed onto different atmospheric variables to study the underlying physical processes at work, showing the spatial dependence of the large-scale climate variability in the Mediterranean region.

By construction of our CCA approach, we addressed multicollinearity between the SST-related individual EV variables. This is the case of AMV and Mediterranean decadal SST variability, for which the time series of their respective indices showed high significant correlation. Thus, and based on previous studies, we assumed that decadal SST variability in both basins is coupled (Marullo et al. 2011; Skliris et al. 2012; Mariotti and Dell'Aquila 2012; Ruprich-Robert et al. 2017), defining the Atlantic-Mediterranean decadal SST variability (AMDV), and associating the region's PCP and TEMP internal variability with a single SST index. Our results partially support the findings of Dünkeloh and Jacobeit (2003), and Xoplaki et al. (2004). They applied CCA to identify main coupled circulation-rainfall patterns on decadal and longer time scales for a relatively short period (1948–98 and 1950–99 respectively), suggesting that variations in Mediterranean winter rainfall were basically influenced by the NAO, consistent with the idea that observed precipitation trends are in part dynamically induced. In a similar framework, Mariotti and Dell'Aquila (2012) showed that over 30% of decadal precipitation variance in zones of the Mediterranean region can be explained by the NAO in DJF, whereas, contrary to our findings, they did not find a significant influence of NAO on decadal TEMP anomalies during winter. This fact reveals the effect of AMDV as a key factor in triggering an effective TEMP response to the NAO in the winter peak season, which would be consistent with Ting et al. (2011), who computed the winter (NDJF) surface temperature projection onto the AMV index and showed that during the warm phase of the AMV, the eastern Mediterranean and Middle East warm up, while the western Mediterranean cools.

Given the prominent roles of DNAO and AMDV, it should be noted that several studies showed a lagged

connection between both phenomena (see the review of Zhang et al. 2019 and citations therein). This DNAO-AMV association is seen in most coupled models of the CMIP5 preindustrial ensemble (which was forced with constant preindustrial, external radiative forcing), though the AMV-DNAO link is commonly stronger in observations (Peings et al. 2016; O'Reilly and Zanna 2018). Be that as it may, our results show that the significant impacts of DNAO and AMDV on Mediterranean hydroclimate variability are independent of the optimum (lagged) NAO-AMV link, in a way that significant TEMP and PCP responses occur when both indices are close to linear independence (i.e., uncorrelated). Thus, the contemporaneous impact is reinforced.

Lastly, while Dong and Dai (2015) found a negative correlation between the IPO and annual temperatures in the Mediterranean Middle East using observations, reanalysis and model simulations, we did not find the IPO to exert a significant influence on TEMP variability. This fact may be due to the annual nature of their study compared to the 3-month fall to spring periods addressed in this work, pointing out the need to further investigate the variations of the Mediterranean TEMP response to IPO on a monthly basis. As for PCP, the role of the IPO in recent tropical widening has been proposed (Allen and Kovilakam 2017), being associated with poleward migration of subtropical dry zones and large-scale atmospheric circulation, especially in the Northern Hemisphere. Nevertheless, we did not notice a significant IPO contribution to the canonical modes associated with a northward shift of the subtropical dry zone, which were otherwise governed by anthropogenic forcing, even though the IPO could play a subsidiary role in terms of multi-decadal variability underlying clear positive long-term trends.

Appendix

Key concepts in CCA

According to the literature (see e.g., Hair et al. 2010), the key concepts to analyze and interpret individual contributions derived from CCA results are defined as follows:

- Canonical coefficients. Parameters that give the contribution of the individual variables within the EV and RV sets to their corresponding canonical variate. These coefficients are equivalent to regression coefficients in multiple linear regression.
- Canonical variates. Time series that represent the linear combination (weighted sum) of two or more variables. These time series are defined for EV and RV.
- Canonical modes. Pairs of canonical variates, one for the set of EV and one for the set of RV. The strength of the link is given by canonical correlation.
- Canonical correlation. Measure of the strength of the relationship between the canonical variates for a given canonical mode. In effect, it represents the bivariate correlation between the two canonical variates.
- Shaded variance. Measure of the variance explained between canonical variates. It is calculated as the squared canonical correlation.
- Canonical loadings. Measure of the simple linear correlation between the individual variables within EV and RV sets and their respective canonical variates.
- Canonical cross-loadings. Correlation of each individual EV or RV with the opposite canonical variate. In other words, the individual EVs are correlated with the RV canonical variate and vice versa.

Individual contributions to canonical modes

The interpretation of canonical variates in a significant canonical mode is based on individual variables (PCs) within the EV and RV sets that contribute markedly to shared variances (i.e., R^2). We restrict our attention to canonical modes by a series of criteria, which are (1) the level of statistical significance of the canonical correlation associated with a given canonical mode and its associated shared variance (i.e., squared canonical correlation), (2) canonical RV loadings, and (3) canonical EV cross-loadings. It is worth noting that canonical coefficients are traditionally used to examine the contribution of individual variables. Nevertheless, its utilization to interpret the relative importance of a variable is subject to criticism in the same way as beta coefficients in conventional regression techniques (Lambert and Durand 1975).

The level of significance for canonical correlations is set in this work at 0.05 (95%), which is the generally accepted level for considering a correlation coefficient statistically significant. We use the Wilks' Lambda as a measure for assessing the significance of discriminant functions (Wilks 1935; Bartlett 1947). The Wilks' Lambda likelihood ratio is a consistent test statistic under the classical assumptions that all groups arise from multivariate normal distributions (e.g., Nath and Pavur 1985; Friederichs and Hense 2003). It tests how well each level of EV contributes to the model. The scale ranges from 0 to 1, where 0 means total discrimination, and 1 means no discrimination. The null hypothesis should be rejected when Wilks' lambda is close to zero in combination with a small p-value (0.05 or lower). The p-values are calculated from an F-statistic, based on Rao's approximation (Bartlett 1941) to evaluate the significance of Wilks' Lambda.

Once a given canonical mode is found to be robust in terms of its significant canonical correlation, the relative relevance of the original variables in the canonical mode involves the calculation of canonical loadings and cross-loadings. The canonical loading is interpreted as the relative contribution of each variable to the canonical mode. It takes into account each independent canonical mode and calculates the within-set variable-to-variate correlation. As for canonical cross-loadings, their calculation has been proposed as a complement to canonical loadings (Dillon and Goldstein 1984). This method implies the calculation of each original EV with the canonical RV variate, and vice versa. Therefore, cross-loadings provide the cross-set variable-to-variate correlation. We evaluate significant individual contributions in terms of canonical RV loadings and canonical EV cross-loadings. The significance level for canonical loadings and cross-loadings is tested by means of the Ebisuzaki's method (Ebisuzaki 1997), which applies to time series that exhibit non-white spectra, or what is the same, time series that violate the assumption of independence that is fundamental to the classical t-test. The Ebisuzaki method consists of a non-parametric test based on generating a large number of random series (permutations) with the same power spectra as the original series but with random phases in the Fourier modes. The number of permutations in this study has been set to 1000.

When all the criteria of statistical significance described above are met, the acceptance of a canonical mode is restricted to the variance explained in the time series of the original anomalous field at each point in space by the canonical EV variate. It may be the case that all the criteria of statistical significance are met but the canonical EV variate is not representative of variability over the original field. In this case, the canonical mode is interpreted as a statistical artifact. This could be related to a negligible contribution of the leading PCs to the canonical RV variates (i.e., non-significant canonical RV loadings). We discard certain PCP and TEMP canonical modes because the characterization of the canonical variates (i.e., the evolution of the time series according to consecutive 3-month periods) is not coherent with the previous or subsequent canonical modes. This does not necessarily imply that the discarded modes do not involve physical causality. Canonical modes discarded according to one or more criteria can be seen in the supplementary material (Figs. S1, S2 and S3).

Variance inflation factor

The variance inflation factor (VIF) is a common collinearity diagnostic (e.g., Rawlings et al. 1998; James et al. 2017). In general, the VIF for the ith regression coefficient can be computed as:

$$VIF_i = \frac{1}{1 - R_i^2} \tag{A1}$$

where R_i^2 is the coefficient of multiple determination obtained by regressing each individual within-set variable onto the remaining variables. When the variation of the i^{th} single variable is largely explained by a linear combination of the remaining variables, R_i^2 is close to 1, and the VIF for that variable is correspondingly large. The inflation is measured relative to an R_i^2 of 0 (VIF of 1; no collinearity). VIFs are also the diagonal elements of the inverse of the correlation matrix (Belsley et al. 1980), a convenient result that eliminates the need to set up the various regressions. There are no statistical tests to rate for multicollinearity using the tolerance of VIF measures. Some authors use a VIF of 10 (inflates the standard error by 3.16) as a suggested upper limit to indicate a definite multicollinearity problem for an individual variable (e.g., Kutner et al. 2004; Zuur et al. 2010). More robustly, a VIF of 4 doubles the standard error. Without an established guidance to adopt a definite value, the tolerance of VIF is subject to the scope of the research problem being addressed.

Supplementary Information The online version contains supplementary material available at https://doi.org/10.1007/s00382-021-05765-1.

Acknowledgements The research leading to this work was supported by the National Science Foundation (NSF Award AGS-1734760). We also thank the editor and three anonymous reviewers for their pertinent comments and suggestions, which have contributed to improve this manuscript. Lamont-Doherty Earth Observatory Contribution Number 8497.

Author contributions RS-M has designed and written the article, and performed the calculations. YK has defined and supervised the application of the methodology. RS has directed and coordinated the work, focusing primarily on results related to large-scale atmospheric dynamics. The three authors have maintained constant feedback and discussion throughout the work.

Funding This work was developed as part of the project "Mechanisms of Mediterranean region hydroclimate variability and change", which is supported by the National Science Foundation (NSF Award AGS-1734760).

Data availability Not applicable.

Code availability Not applicable.

Declarations

Conflicts of interest The authors declare no conflict of interest.

References

Allen RJ, Kovilakam M (2017) The role of natural climate variability in recent tropical expansion. J Clim 30:6329–6350. https://doi.org/10.1175/JCLI-D-16-0735.1

Årthun M, Kolstad EW, Eldevik T, Keenlyside NS (2018) Time scales and sources of European temperature variability. Geophys Res Lett 45:3597–3604. https://doi.org/10.1002/2018GL077401

Baines PG, Folland CK (2007) Evidence for a rapid global climate shift across the late 1960s. J Clim 20:2721–2744. https://doi.org/10.1175/JCLI4177.1

Barnett TP, Preisendorfer R (1987) Origins and levels of monthly and seasonal forecast skill for united states surface air temperatures determined by canonical correlation analysis. Mon Wea Rev 115:1825–1850. https://doi.org/10.1175/1520-0493(1987)115%3c1825:OALOMA%3e2.0.CO;2

Bartlett MS (1941) The statistical significance of canonical correlations. Biometrika 32:29–37

Bartlett MS (1947) Multivariate analysis. Suppl J R Stat Soc 9(2):176–197

Belsley DA, Kuh E, Welsch RE (1980) Identifying influential data and sources of collinearity. Wiley, New York

Bretherton CS, Smith C, Wallace JM (1992) An intercomparison of methods for finding coupled patterns in climate data. J Clim 5:541–560. https://doi.org/10.1175/15200442(1992)005%3c0541:AIOMFF%3e2.0.CO;2

Cayan DR (1992) Latent and sensible heat flux anomalies over the northern oceans: driving the sea surface temperature. J Phys Oceanogr 22:859–881. https://doi.org/10.1175/1520-0485(1992)022%3c0859:LASHFA%3e2.0.CO;2

Collins WD et al (2006) Radiative forcing by well-mixed greenhouse gases: estimates from climate models in the intergovernmental panel on climate change (IPCC) fourth assessment report (AR4). J Geophys Res 111:D14317. https://doi.org/10.1029/2005JD006713

Compo GP et al (2011) The twentieth century reanalysis project. Q J R Meteorol Soc 137(654):1–28

Comrie AC, Glenn EC (1998) Principal components-based regionalization of precipitation regimes across the southwest United States and northern Mexico, with an application to monsoon precipitation variability. Clim Res 10:201–215

Cook KH (2004) Hadley circulation dynamics: seasonality and the role of continents in the hadley circulation: present, past and future. pp. 61–83. Springer, New York, USA. doi:https://doi.org/10.1007/978-1-4020-2944-8_2.

Cramer W, Guiot J, Fader M et al (2018) Climate change and interconnected risks to sustainable development in the Mediterranean. Nat Clim Change 8:972–980. https://doi.org/10.1038/s41558-018-0299-2

Czaja A, Robertson AW, Huck T (2003) The role of Atlantic ocean-atmosphere coupling in affecting North Atlantic Oscillation Variability. In: Hurrell JW, Kushnir Y, Ottersen G, Visbeck M (eds) The North Atlantic Oscillation: climatic significance and environmental impact. Geophys Monogr 134: 147–172

de Haas H (2011) Mediterranean migration futures: patterns, drivers and scenarios. Global Environ Change 21:S59–S69. https://doi.org/10.1016/j.gloenvcha.2011.09.003

Delworth TL, Zeng F, Zhang L, Zhang R, Vecchi GA, Yang X (2017) The central role of ocean dynamics in connecting the North Atlantic oscillation to the extratropical component of the atlantic multidecadal oscillation. J Clim 30:3789–3805. https://doi.org/10.1175/JCLI-D-16-0358.1

Deser C, Alexander MA, Xie SP, Phillips AS (2010) Sea surface temperature variability: patterns and mechanisms. Annu Rev Mar Sci 2:115–143. https://doi.org/10.1146/annurev-marine-120408-151453

Dillon WR, Goldstein M (1984) Multivariate analysis. Wiley, New York

Dong B, Dai A (2015) The influence of the interdecadal pacific oscillation on temperature and precipitation over the globe. Clim Dyn 45:2667–2681. https://doi.org/10.1007/s00382-015-2500-x

Dünkeloh A, Jacobeit J (2003) Circulation dynamics of Mediterranean precipitation variability 1948–98. Int J Climatol 23:1843–1866. https://doi.org/10.1002/joc.973

Ebisuzaki W (1997) A method to estimate the statistical significance of a correlation when the data are serially correlated. J Clim 10:2147–2153. https://doi.org/10.1175/1520-0442(1997)010%3c2147:AMTETS%3e2.0.CO;2

Enfield DB, Mestas-Nuñez AM, Trimble PJ (2001) The Atlantic Multidecadal Oscillation and its relation to rainfall and river flows in the continental US. Geophys Res Lett 28:2077–2080

Feldman D, Collins W, Gero P, Torn MS, Mlawer EJ, Shippert TR (2015) Observational determination of surface radiative forcing by CO_2 from 2000 to 2010. Nature 519:339–343. https://doi.org/10.1038/nature14240

Friederichs P, Hense A (2003) Statistical inference in canonical correlation analyses exemplified by the influence of North Atlantic SST on european climate. J Climate 16:522–534. https://doi.org/10.1175/1520-0442(2003)016%3c0522:SIICCA%3e2.0.CO;2

García-Serrano J, Polo I, Rodríguez-Fonseca B, Losada T (2013) Large-scale atmospheric response to eastern Mediterranean summer-autumn SST anomalies and the associated regional impact. Clim Dyn 41:2251–2265. https://doi.org/10.1007/s00382-013-1940-4

Gastineau G, Le Treut H, Li L (2008) Hadley circulation changes under global warming conditions indicated by coupled climate models. Tellus A 60(5):863–884. https://doi.org/10.1111/j.1600-0870.2008.00344.x

Ghosh R, Müller WA, Baehr J, Bader J (2017) Impact of observed North Atlantic multidecadal variations to European summer climate: a linear baroclinic response to surface heating. Clim Dyn 48:3547–3563. https://doi.org/10.1007/s00382-016-3283-4

Green PE (1978) Analyzing Multivariate Data. Holt, Rinehart & Winston, Illinois, USA

Green PE, Carroll JD (1978) Mathematical tools for applied multivariate analysis. Academic Press, New York

Grise KM et al (2019) Recent tropical expansion: natural variability or forced response? J Clim 32:1551–1571. https://doi.org/10.1175/JCLI-D-18-0444.1

Hair J, Black W, Babin B, Anderson R (2010) Multivariate data analysis (7th ed.): Upper Saddle River, NJ, USA: Prentice-Hall, Inc.

Hamann A, Wang T (2006) Potential effects of climate change on ecosystem and tree species distribution in British Columbia. Ecology 87:2773–2786

Harris I, Osborn TJ, Jones P, Lister D (2020) Version 4 of the CRU TS monthly high-resolution gridded multivariate climate dataset. Sci Data 7:109. https://doi.org/10.1038/s41597-020-0453-3

Hu Y, Fu Q (2007) Observed poleward expansion of the Hadley circulation since 1979. Atmos Chem Phys 7:5229–5236

Hu Y, Tao L, Liu J (2013) Poleward expansion of the hadley circulation in CMIP5 simulations. Adv Atmos Sci 30:790–795. https://doi.org/10.1007/s00376-012-2187-4

Huang B, Thorne PW, Banzon VF, Boyer T, Chepurin G, Lawrimore JH, Menne MJ, Smith TM, Vose RS, Zhang H (2017) Extended reconstructed sea surface temperature, version 5 (ERSSTv5): upgrades, validations, and intercomparisons. J Clim 30:8179–8205. https://doi.org/10.1175/JCLI-D-16-0836.1

Hurrell JW (1995) Decadal trends in the North Atlantic oscillation: regional temperatures and precipitation. Science 269(5224):676–679

Hurrell JW, Deser C (2009) North Atlantic climate variability: the role of the North Atlantic Oscillation. J Mar Syst 78:28–41. https://doi.org/10.1016/j.jmarsys.2008.11.026

Hurrell JW, Kushnir Y, Visbeck M (2001) The North Atlantic oscillation. Science 291:603–605. https://doi.org/10.1126/science.1058761

Hurrell JW, Kushnir Y, Visbeck M, Ottersen G (2003) An overview of the North Atlantic oscillation. The North Atlantic oscillation: climate significance and environmental impact, Geophys Monogr. Vol. 134, Amer. Geophys. Union, 1–35.

IPCC (2018) Global Warming of 1.5°C. An IPCC Special Report on the impacts of global warming of 1.5°C above pre-industrial levels and related global greenhouse gas emission pathways, in the context of strengthening the global response to the threat of climate change, sustainable development, and efforts to eradicate poverty. Masson-Delmotte V, Zhai P, Pörtner HO, Roberts D, Skea J, Shukla PR, Pirani A, Moufouma-Okia W, Péan C, Pidcock R, Connors S, Matthews JBR, Chen Y, Zhou X, Gomis MI, Lonnoy E, Maycock T, Tignor M, Waterfield T (eds.).

Jain AK, Briegleb BP, Minschwaner K, Wuebbles DJ (2000) Radiative forcings and global warming potentials of 39 greenhouse gases. J Geophys Res. 105(D16), 20773– 20790, doi:https://doi.org/10.1029/2000JD900241.

James G, Witten D, Hastie T, Tibshirani R (2017) An introduction to statistical learning (8th ed.). Springer Science+Business Media New York. ISBN: 978-1-4614-7138-7

Jones PD, Jonsson T, Wheeler D (1997) Extension to the North Atlantic oscillation using early instrumental pressure observations from Gibraltar and south-west Iceland. Int J Climatol 17:1433–1450. https://doi.org/10.1002/(SICI)1097-0088(19971115)17:13%3c1433::AID-JOC203%3e3.0.CO;2-P

Kelley C, Ting M, Seager R, Kushnir Y (2012a) Mediterranean precipitation climatology, seasonal cycle, and trend as simulated by CMIP5. Geophys Res Lett 39:L21703. https://doi.org/10.1029/2012GL053416

Kelley C, Ting M, Seager R, Kushnir Y (2012b) The relative contributions of radiative forcing and internal climate variability to the late 20th Century winter drying of the Mediterranean region. Clim Dyn 38:2001–2015. https://doi.org/10.1007/s00382-011-1221-z

Kelley C, Mohtadi S, Cane MA, Seager R, Kushnir Y (2015) Climate change in the ent and implications of the recent Syrian drought. Proc Natl Acad Sci USA 112(11):3241–3246. https://doi.org/10.1073/pnas.1421533112

Knight JR, Folland CK, Scaife AA (2006) Climate impacts of the Atlantic multidecadal oscillation. Geophys Res Lett 33:L17706. https://doi.org/10.1029/2006GL026242

Kottek M, Grieser J, Beck C, Rudolf B, Rubel F (2006) World Map of the Köppen-Geiger climate classification updated. Meteorologishe Zeitschrift 15:259–263

Kushnir Y (1994) Interdecadal variations in North atlantic sea surface temperature and associated atmospheric conditions. J Clim 7:141–157. https://doi.org/10.1175/1520-0442(1994)007%3c0141:IVINAS%3e2.0.CO;2

Kutner MH, Nachtsheim CJ, Neter J (2004) Applied Linear Regression Models (4thed.). Homewood, IL: Irwin.

Lambert ZV, Durand RM (1975) Some precautions in using canonical analysis. J Mark Res 12:468–475

Lashof DA, Ahuja DR (1990) Relative contributions of greenhouse gas emissions to global warming. Nature 344(6266):529–531. https://doi.org/10.1038/344529a0

Li L (2006) Atmospheric GCM response to an idealized anomaly of the Mediterranean sea surface temperature. Clim Dyn 27:543–552. https://doi.org/10.1007/s00382-006-0152-6

Li J, Sun C, Jin FF (2013) NAO implicated as a predictor of Northern Hemisphere mean temperature multidecadal variability. Geophys Res Lett 40:5497–5502. https://doi.org/10.1002/2013GL057877

Lionello P, Scarascia L (2018) The relation between climate change in the Mediterranean region and global warming. Reg Environ Change 18:1481–1493. https://doi.org/10.1007/s10113-018-1290-1

Lu J, Greatbatch RJ, Peterson KA (2004) Trend in Northern hemisphere winter atmospheric circulation during the last half of the twentieth century. J Clim 17:3745–3760. https://doi.org/10.1175/1520-0442(2004)017%3c3745:TINHWA%3e2.0.CO;2

Lu J, Vecchi GA, Reichler T (2007) Expansion of the Hadley cell under global warming. Geophys Res Lett 34(6):L06805. https://doi.org/10.1029/2006GL028443

Mann ME (2004) On smoothing potentially non-stationary climate time series. Geophys Res Lett 31:L07214. https://doi.org/10.1029/2004GL019569

Mann ME (2008) Smoothing of climate time series revisited. Geophys Res Lett 35:L16708. https://doi.org/10.1029/2008GL034716

Mariotti A, Dell'Aquila A (2012) Decadal climate variability in the Mediterranean region: roles of large-scale forcings and regional processes. Clim Dyn 38:1129–1145. https://doi.org/10.1007/s00382-011-1056-7

Mariotti A, Ballabrera-Poy J, Zeng N (2005) Tropical influence on Euro-Asian autumn rainfall variability. Clim Dyn 24:511–521. https://doi.org/10.1007/s00382-004-0498-6

Mariotti A, Zeng N, Lau KM (2002) Euro-Mediterranean rainfall and ENSO—a seasonally varying relationship. Geophys Res Lett 29(12). https://doi.org/10.1029/2001GL014248

Marullo S, Artale V, Santoleri R (2011) The SST Multidecadal variability in the atlantic-mediterranean region and its relation to AMO. J Clim 24:4385–4401. https://doi.org/10.1175/2011JCLI3884.1

Maslova VM, Voskresenskaya EN, Lubkov AS (2017) Multidecadal change of winter cyclonic activity in the Mediterranean associated with AMO and PDO. Terr Atmos Ocean Sci 28(2017):965–977. https://doi.org/10.3319/TAO.2017.04.23.01

McCarthy G, Haigh I, Hirschi J, Grist P, Smeed A (2015) Ocean impact on decadal Atlantic climate variability revealed by sea-level observations. Nature 521:508–510. https://doi.org/10.1038/nature14491

Meehl GA, Hu A, Arblaster JM, Fasullo J, Trenberth KE (2013) Externally forced and internally generated decadal climate variability associated with the interdecadal pacific oscillation. J Clim 26:7298–7310. https://doi.org/10.1175/JCLI-D-12-00548.1

Mohino E, Janicot S, Bader J (2011) Sahel rainfall and decadal to multi-decadal sea surface temperature variability. Clim Dyn 37:419–440. https://doi.org/10.1007/s00382-010-0867-2

Mohino E, Keenlyside N, Pohlmann H (2016) Decadal prediction of Sahel rainfall: where does the skill (or lack thereof) come from? Clim Dyn 47:3593–3612. https://doi.org/10.1007/s00382-016-3416-9

Myhre G, Highwood EJ, Shine KP, Stordal F (1998) New estimates of radiative forcing due to well mixed greenhouse gases. Geophys Res Lett 25:2715–2718

Nath R, Pavur R (1985) A new statistic in the one way multivariate analysis of variance. Comput Stat Data An 2(4):297–315

O'Reilly CH, Woollings T, Zanna L (2017) The dynamical influence of the atlantic multidecadal oscillation on continental climate. J Clim 30:7213–7230. https://doi.org/10.1175/JCLI-D-16-0345.1

O'Reilly CH, Zanna L (2018) The signature of oceanic processes in decadal extratropical SST anomalies. Geophys Res Lett 45:7719–7730. https://doi.org/10.1029/2018GL079077

Peings Y, Simpkins G, Magnusdottir G (2016) Multidecadal fluctuations of the North Atlantic Ocean and feedback on the winter climate in CMIP5 control simulations. J Geophys Res Atmos 121:2571–2592. https://doi.org/10.1002/2015JD024107

Qasmi S, Cassou C, Boé J (2017) teleconnection between atlantic multidecadal variability and european temperature: diversity and evaluation of the coupled model intercomparison project phase 5 models. Geophys Res Lett. 44, 11,140– 11,149. https://doi.org/https://doi.org/10.1002/2017GL074886

Rawlings JO, Pantula SG, Dickey AD (1998) Applied regression analysis. Springer, New York

Ruprich-Robert Y, Msadek R, Castruccio F, Yeager S, Delworth T, Danabasoglu G (2017) Assessing the Climate Impacts of the Observed Atlantic Multidecadal Variability Using the GFDL CM2.1 and NCAR CESM1 Global Coupled Models. J Clim. 30(8), 2785–2810. http://journals.ametsoc.org/doi/abs/https://doi.org/10.1175/JCLI-D-16-0127.1

Scheutz C, Kjeldsen P, Gentil E (2009) Greenhouse gases, radiative forcing, global warming potential and waste management—an introduction. Waste Manage Res. 27 (8) (September 2009), pp. 716–723

Schlesinger ME, Ramankutty N (1994) An oscillation in the global climate system of period 65–70 years. Nature 367:723–726

Schneider U, Becker A, Finger P, Meyer-Christoffer A, Ziese M, Rudolf B (2013) GPCC's new land surface precipitation climatology based on quality-controlled in situ data and its role in quantifying the global water cycle. Theor Appl Climatol 115:15–40. https://doi.org/10.1007/s00704-013-0860-x

Seager R, Kushnir Y, Visbeck M, Naik N, Miller J, Krahmann G, Cullen H (2000) Causes of Atlantic Ocean climate variability between 1958 and 1998. J Clim 13:2845–2862. https://doi.org/10.1175/1520-0442(2000)013%3c2845:COAOCV%3e2.0.CO;2

Seager R, Liu H, Henderson N, Simpson I, Kelley C, Shaw T, Kushnir Y, Ting M (2014) Causes of increasing aridification of the mediterranean region in response to rising greenhouse gases. J Clim 27:4655–4676. https://doi.org/10.1175/JCLI-D-13-00446.1

Seager R, Osborn TJ, Kushnir Y, Simpson I, Nakamura J, Liu H (2019) Climate variability and change of mediterranean-type climates. J Clim 32:2887–2915. https://doi.org/10.1175/JCLI-D-18-0472.1

Seager R, Liu H, Kushnir Y, Osborn TJ, Simpson I, Kelley C, Nakamura J (2020) Mechanisms of winter precipitation variability in the European-Mediterranean region associated with the North Atlantic Oscillation. (under review in J Clim)

Simpson I, Seager R, Ting M, Shaw T (2016) Causes of change in Northern Hemisphere winter meridional winds and regional hydroclimate. Nature Clim Change 6:65–70. https://doi.org/10.1038/nclimate2783

Skliris N, Sofianos S, Gkanasos A, Mantziafou A, Vervatis V, Axaopoulos P, Lascaratos A (2012) Decadal scale variability of sea surface temperature in the Mediterranean Sea in relation to atmospheric variability. Ocean Dyn 62:13–30. https://doi.org/10.1007/s10236-011-0493-5

Slivinski LC, Compo GP, Whitaker JS et al (2019) Towards a more reliable historical reanalysis: improvements for version 3 of the twentieth century reanalysis system. Q J R Meteorol Soc 145:2876–2908. https://doi.org/10.1002/qj.3598

Somot S, Sevault F, Deque M, Crepon M (2008) 21st century climate change scenario for the Mediterranean using a coupled atmosphere-ocean regional climate model. Global Planet Change 63:112–126

Sun C, Li J, Jin F (2015) A delayed oscillator model for the quasi-periodic multidecadal variability of the NAO. Clim Dyn 45:2083–2099. https://doi.org/10.1007/s00382-014-2459-z

Sun Q, Miao C, Duan Q, Ashouri H, Sorooshian S, Hsu KL (2018) A review of global precipitation data sets: data sources, estimation, and intercomparisons. Rev Geophys 56:79–107. https://doi.org/10.1002/2017RG000574

Sutton RT, Hodson DLR (2005) Atlantic ocean forcing of North American and European summer climate. Science 309:115–118

Sutton RT, Dong B (2012) Atlantic Ocean influence on a shift in European climate in the 1990s. Nat Geosci 5:788–792. https://doi.org/10.1038/NGEO1595

Tang T, Shindell D, Samset BH, Boucher O, Forster PM, Hodnebrog Ø et al (2018) Dynamical response of Mediterranean precipitation to greenhouse gases and aerosols. Atmos Chem Phys 18(11):8439–8452. https://doi.org/10.5194/acp-18-8439-2018

Tao L, Hu Y, Liu J (2016) Anthropogenic forcing on the Hadley circulation in CMIP5 simulations. Clim Dyn 46:3337–3350. https://doi.org/10.1007/s00382-015-2772-1

Thompson B (2000) Canonical correlation analysis. In: Grimm L, Yarnold P (eds) Reading and understanding more multivariate statistics. American Psychological Association, Washington, pp 285–316

Ting M, Kushnir Y, Seager R, Li C (2009) Forced and internal twentieth-century SST Trends in the North Atlantic. J Clim 22:1469–1481. https://doi.org/10.1175/2008JCLI2561.1

Ting M, Kushnir Y, Seager R, Li C (2011) Robust features of Atlantic multidecadal variability and its climate impacts. Geophys Res Lett 38:L17705. https://doi.org/10.1029/2011GL048712

Trenberth KE, Shea DJ (2006) Atlantic hurricanes and natural variability in 2005. Geophys Res Lett 33:L12704. https://doi.org/10.1029/2006GL026894

Visbeck MH, Hurrell JW, Polvani L, Cullen HM (2001) Proc Natl Acad Sci 98(23):12876–12877. https://doi.org/10.1073/pnas.231391598

Visbeck M, Chassignet E, Curry R, Delworth T (2003) The ocean's response to North Atlantic variability. The North Atlantic oscillation, In: Hurrell J, Kushnir Y, Ottersen G, Visbeck M (eds) Geophysical monograph, vol 134. American Geophysical Union, pp 113–145

Wang S, Huang J, He Y, Guan Y (2014) Combined effects of the Pacific decadal oscillation and El Nino-southern oscillation on global land dry–wet changes. Sci Rep 4:6651. https://doi.org/10.1038/srep06651

Widmann M (2005) One-Dimensional CCA and SVD, and Their Relationship to Regression Maps, J Clim. 18(14), 2785–2792. https://journals.ametsoc.org/view/journals/clim/18/14/jcli3424.1.xml

Wilks SS (1935) On the independence of k sets of normally distributed statistical variables. Econometrica 3(3):309–326. https://doi.org/10.2307/1905324

Wilks DS (1995) Statistical methods in the atmospheric sciences: an introduction. Academic Press, 467 pp.

Xoplaki E, González-Rouco JF, Luterbacher J, Wanner H (2004) Wet season Mediterranean precipitation variability: influence of large-scale dynamics and trends. Clim Dyn 23:63–78. https://doi.org/10.1007/s00382-004-0422-0

Zampieri M, Toreti A, Schindler A, Scoccimarro E, Gualdi S (2017) Atlantic multidecadal oscillation influence on weather regimes over Europe and the Mediterranean in spring and summer. Global Planet Change 151:92–100. https://doi.org/10.1016/j.gloplacha.2016.08.014

Zappa G, Hoskins BJ, Shepherd TG (2015) The dependence of wintertime Mediterranean precipitation on the atmospheric circulation response to climate change. Environ Res Lett 10:104012. https://doi.org/10.1088/17489326/10/10/104012

Zhang R, Delworth TL, Held IM (2007) Can the Atlantic Ocean drive the observed multidecadal variability in Northern Hemisphere mean temperature? Geophys Res Lett 34:L02709. https://doi.org/10.1029/2006GL028683

Zhang R, Sutton R, Danabasoglu G, Kwon YO, Marsh R, Yeager SG, Amrhein DE, Little CM (2019) A review of the role of the

atlantic meridional overturning circulation in atlantic multidecadal variability and associated climate impacts. Rev Geophys 57:316–375. https://doi.org/10.1029/2019RG000644

Zittis G (2018) Observed rainfall trends and precipitation uncertainty in the vicinity of the Mediterranean, Middle East and North Africa. Theor Appl Climatol 134:1207–1230. https://doi.org/10.1007/s00704-017-2333-0

Zittis G, Hadjinicolaou P, Klangidou M, Proestos Y, Lelieveld J (2019) A multi-model, multi-scenario, and multi-domain analysis of regional climate projections for the Mediterranean. Reg Environ Chang 19:2621–2635. https://doi.org/10.1007/s10113-019-01565-w

Zuur AF, Ieno EN, Elphick CS (2010) A protocol for data exploration to avoid common statistical problems. Methods Ecol Evol 1:3–14. https://doi.org/10.1111/j.2041-210X.2009.00001.x